Available online at www.sciencedirect.com
SCIENCE DIRECT®
Applied Geochemistry 20 (2005) 639–659
Applied Geochemistry
www.elsevier.com/locate/apgeochem

Release, transport and attenuation of metals from an old tailings impoundment

M.C. Moncur [a], C.J. Ptacek [a,b,*], D.W. Blowes [a], J.L. Jambor [c]

[a] Department of Earth Sciences, University of Waterloo, 200 University Avenue, Waterloo, Ont., Canada N2L 3G1
[b] National Water Research Institute, Environment Canada, 867 Lakeshore Road, P.O. Box 5050, Burlington, Ont., Canada L7R 4A6
[c] Department of Earth and Ocean Sciences, University of British Columbia, 6339 Stores Road, Vancouver, BC, Canada V6T 1Z4

Received 24 May 2004; accepted 25 September 2004
Editorial handling by R. Fuge

Abstract

The oxidation of sulfide minerals from mine wastes results in the release of oxidation products to groundwater and surface water. The abandoned high-sulfide Camp tailings impoundment at Sherridon, Manitoba, wherein the tailings have undergone oxidation for more than 70 a, was investigated by hydrogeological, geochemical, and mineralogical techniques. Mineralogical analysis indicates that the unoxidized tailings contain nearly equal proportions of pyrite and pyrrhotite, which make up to 60 wt% of the total tailings, and which are accompanied by minor amounts of chalcopyrite and sphalerite, and minute amounts of galena and arsenopyrite. Extensive oxidation in the upper 50 cm of the tailings has resulted in extremely high concentrations of dissolved SO_4 and metals and As in the tailings pore water (pH < 1, 129,000 mg L^{-1} Fe, 280,000 mg L^{-1} SO_4, 55,000 mg L^{-1} Zn, 7200 mg L^{-1} Al, 1600 mg L^{-1} Cu, 260 mg L^{-1} Mn, 110 mg L^{-1} Co, 97 mg L^{-1} Cd, 40 mg L^{-1} As, 15 mg L^{-1} Ni, 8 mg L^{-1} Pb, and 3 mg L^{-1} Cr). The acid released from sulfide oxidation has been extensive enough to deplete carbonate minerals to 6 m depth and to partly deplete Al-silicate minerals to a 1 m depth. Below 1 m, sulfide oxidation has resulted in the formation of a continuous hardpan layer that is >1 m thick. Geochemical modeling and mineralogical analysis indicate that the hardpan layer consists of secondary melanterite, rozenite, gypsum, jarosite, and goethite. The minerals indicated mainly control the dissolved concentrations of SO_4, Fe, Ca and K. The highest concentrations of dissolved metals are observed directly above and within the massive hardpan layer. Near the water table at a depth of 4 m, most metals and SO_4 sharply decline in concentration. Although dissolved concentrations of metals and SO_4 decrease below the water table, these concentrations remain elevated throughout the tailings, with up to 60,600 mg L^{-1} Fe and 91,600 mg L^{-1} SO_4 observed in the deeper groundwater. During precipitation events, surface seeps develop along the flanks of the impoundment and discharge pore water with a geochemical composition that is similar to the composition of water directly above the hardpan. These results suggest that shallow lateral flow of water from a transient perched water table is resulting in higher contaminant loadings than would be predicted if it were assumed that discharge is derived solely from the deeper primary water table. The abundance of residual sulfide minerals, the depletion of aluminosilicate minerals in the upper meter of the tailings and the presence of a significant mass of residual sulfide minerals in this zone after 70 a of oxidation suggest that sulfide oxidation will continue to release acid, metals, and SO_4 to the environment for decades to centuries.

* Corresponding author. Tel.: +1 519 888 4567; fax: +1 519 746 3882.
E-mail address: ptacek@sciborg.uwaterloo.ca (C.J. Ptacek).

0883-2927/$ - see front matter © 2004 Elsevier Ltd. All rights reserved.
doi:10.1016/j.apgeochem.2004.09.019

1. Introduction

Mining of base and precious metals results in the production of immense quantities of waste rock, mill tailings, and waste related to refining processes. In many cases, waste rock and mill tailings contain an abundance of sulfide minerals, mainly pyrite and pyrrhotite, which are of little economic value. The mine wastes are typically deposited in impoundments or piles. Exposure of the sulfide minerals to atmospheric O_2 may ultimately lead to the formation of acid mine drainage (AMD). AMD is low-pH water that typically contains high concentrations of SO_4, Fe(II) and Fe(III), and other metals. AMD waters may have high concentrations of either Fe(II) or Fe(III) depending on Eh–pH conditions. The oxidation of sulfide minerals within mine wastes and workings may continue to release metals to the surrounding environment for decades to millennia (Blowes et al., 1992; Nordstrom and Alpers, 1999; Pyatt and Grattan, 2001). Studies of soils adjacent to ancient mining wastes in southern Jordan revealed high concentrations of metals (12 $g\,kg^{-1}$ Cu and 15 $g\,kg^{-1}$ Pb) despite 2 Ka of weathering (Pyatt et al., 2000).

Studies of the mobilization of metals from very old tailings require information on the milling and refining processes, which can affect the type of mine waste generated. Refining and milling methods prior to 1874 consisted of the crude crushing and smelting of ore, beneficiation procedures that had remained almost unchanged since the days of Agricola in the 16th century (Djingheuzian, 1957). Most AMD would have resulted from the weathering of waste rock, mine workings, and ore rejects and refining products. The invention of the Frue vanner in 1874 made it possible to concentrate lower grade base-metal ores that were not directly smelted, resulting in the generation of fine-grained tailings. At the close of the 19th century, gravity concentration was the dominant method for removal of base metals. However, gravity concentration limited base-metal recoveries typically to within the range of 55–60%, and required for efficiency a minimum production of fines from the milling processes (Djingheuzian, 1957). With the introduction of cyanidation and froth flotation at the beginning of the 20th century, metal recoveries increased by 20–30%, and milling problems became less problematic as a consequence of the more efficient recovery of fines (Coleman and Wallace, 1978).

Flotation and cyanidation allowed the mining of low-grade ore deposits that had been previously uneconomical, and a resulting repercussion was the generation of vast quantities of fine-grained tailings. The fine grain size of mill tailings leads to a large ratio of surface area to mass, hence significantly increasing the availability of sulfide minerals to oxidation. For example, the difference in the ratio of surface area to mass for a particle 1 cm in diameter and a particle of 1 μm diameter is 1 to 10,000 (Meloy, 1962). It was not until 1909 that froth flotation was used in Canada, and by 1920 flotation had become fully established throughout the country (Djingheuzian, 1957).

The Sherritt Gordon mine, at Sherridon, Manitoba, produced some of the first mill tailings in Canada. The tailings are fine-grained: most particles are on the order of 100–200 μm in diameter, although diameters of up to 0.5 mm are common. Detailed field investigations were conducted during the summers of 2000 and 2001 at this site to characterize the tailings solids, pore waters, and groundwater. The objective was to quantify the extent of sulfide oxidation and subsequent release of oxidation products from these early tailings, and to determine the acid-neutralization reactions within the unsaturated zone of the tailings after more than 70 a of weathering.

2. Site description

The Camp tailings impoundment is at Sherridon, Manitoba, 65 km NE of Flin Flon (Fig. 1), which is in a continental high boreal region. The mean annual precipitation of the area (1927–1990) is 485 mm (Environment Canada, 2003) and evapotranspiration is 350 mm (Hydrological Atlas of Canada, 1978). Average monthly temperatures in the area range from −21 °C in January to 18 °C in July (Environment Canada, 2003). The mean annual temperature is 0.5 °C.

The Sherritt Gordon mine consisted of two Precambrian orebodies, each about 5 m thick, that occurred as lenticular layers of massive and disseminated sulfides and as irregular remobilized masses (Goetz and Froese, 1982). The ore averaged 2.45 wt% Cu, 2.97 wt% Zn, 0.62 $g\,t^{-1}$ Au, and 19.9 $g\,t^{-1}$ Ag (Farley, 1949). Ore-zone sulfides were, in decreasing order of abundance, pyrite [FeS_2] and pyrrhotite [$Fe_{1-x}S$] (2:1 ratio), chalcopyrite [$CuFeS_2$], sphalerite [ZnS], and accessory cubanite [$CuFe_2S_3$]. Farley (1949) reported rare arsenopyrite [FeAsS], native Au, and irregular occurrences of galena [PbS] in veinlets and disseminations within hanging-wall shear zones in the gneiss host rock. A total of 7.7 Mt of pyritic ores was milled (Goetz and Froese, 1982), producing 166,093 t of Cu, 135,108 t of 50% Zn concentrate, and minor amounts of Ag (91,320 kg) and Au (2867 kg) (Mineral Resources Branch, 1978).

The Sherritt Gordon mine apparently commenced Cu production in 1928, but operations were suspended in 1932 because of depressed metal markets. Sphalerite was not recovered by the concentrator during the early years of operation because of interferences from fast-floating pyrrhotite (Walker, 1930). Mining and milling were resumed in 1937, but not until 1942 was a Zn concentrate also produced. The mine closed in September 1951 when ore reserves were depleted.

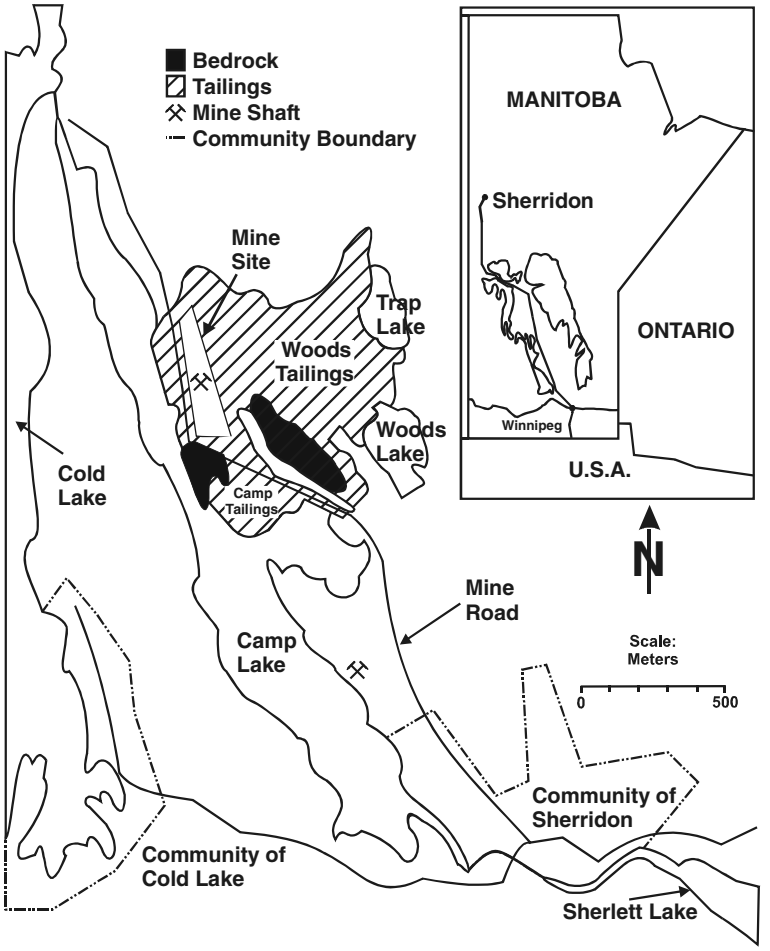

Fig. 1. Location of the Sherridon study area.

Tailings from the Sherritt Gordon mining operations were discharged in two separate tailings impoundments containing a combined 7.4 Mt and occupying an area of 47 ha (Fig. 1). The Camp tailings were discharged into Camp Lake from 1931 to 1932, partly infilling a bay and forming a mounded beach of exposed tailings 7 ha in area. Bedrock underlies the Camp tailings from S4 to near S2 piezometers, and fine-grained lake sediments underlie the tailings between S2 and S1 piezometers (Fig. 2). The Camp tailings have undergone more than 70 a of oxidation. The remaining tailings were deposited in the Woods tailings impoundment and have been exposed to oxidation for more than 50 a. The Woods tailings encompass an area of 40 ha and completely infill Trap Lake and about half of Woods Lake. A NW-trending valley between the former minesite and the Woods tailings separates the two impoundments. In both impoundments a massive (>1 m thick) continuous hardpan layer is present between 0.5 and 2.0 m depth from the tailings surface. The hardpan follows the

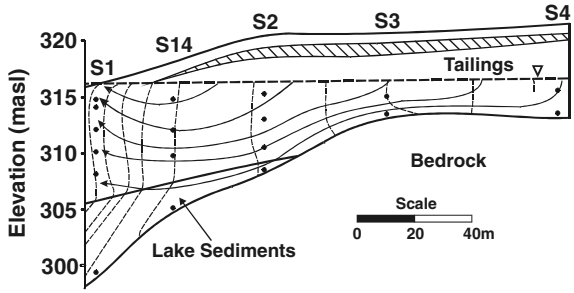

Fig. 2. Transect across the Camp tailings from S1 to S4 piezometers, showing stratigraphy and groundwater flow. Solid lines with arrows are the groundwater flow and the dashed lines are equipotential lines. Black dots represent piezometer sampling locations. Dashed line with inverted triangle represents the water table. The cross-hatched area indicates the extent of the hardpan.

topography of the tailings surface and slopes toward the edges of the impoundment, thereupon pinching out adjacent to surface-water bodies and groundwater discharge zones.

3. Methods

3.1. Piezometer network

The tailings impoundments were instrumented with 5 piezometer nests (Fig. 2), each nest consisting of 2–6 drive-point and (or) bundle piezometers. Fourteen single-point piezometers were installed around the perimeter of the Camp impoundment (Fig. 3). Drive-point piezometers were installed in the tailings by direct-push methods using a gasoline-powered vibrating hammer. Bundle piezometers were installed by pushing to the requisite depth a hollow drill casing with a knock-out tip on the base.

Rising-head piezometer-response tests were performed to estimate the hydraulic conductivity of the tailings. Hydraulic conductivities were calculated using the Hvorslev (1951) method. Hydraulic head measurements were made using a Solinst water-level tape. Water levels were measured in all piezometers on August 3, 2000, on July 10 and 31, August 12, and September 29, 2001, and on June 9 and July 26, 2002.

3.2. Tailings pore gas and solids

Samples of tailings pore gas were collected with drive-point sampling tubes and were analyzed for O_2 in the field using a portable meter, Nova model LBD50. Pore gas was measured at 10 cm increments from the surface of the tailings to the depth of O_2 gas depletion at all piezometer-nest locations.

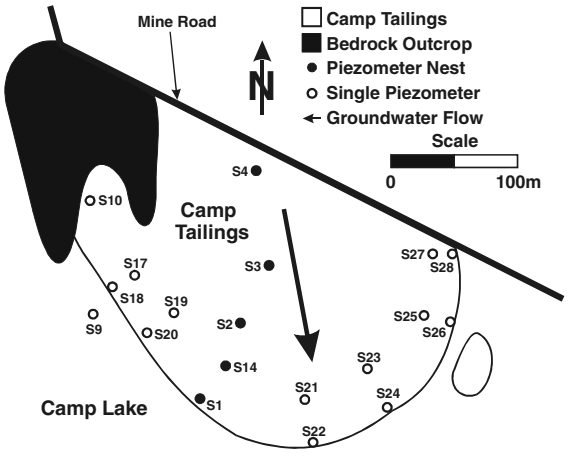

Fig. 3. Location of single drive-point piezometers and piezometer nests installed in the Camp tailings. The bold arrow indicates the average direction of groundwater flow, calculated using the method of Devlin (2003).

At all piezometer-nest locations continuous cores of the tailings were collected from the tailings surface to refusal. Cores were collected in thin-wall Al tubes of 5.1 or 7.6 cm diameter. Where hardpan was encountered, a backhoe was used to excavate a pit through to the underlying unconsolidated tailings. At the bottom of the excavated pit, tailings samples were collected using the piston core-barrel method described by Starr and Ingleton (1992). Samples of hardpan were collected from the walls of the excavated pit by a horizontal coring method using Al tubing of 5.1 or 7.6 cm diameter. All cores were cut into 20–30 cm lengths, then immediately frozen except for the S2 and S3 cores, which were immediately sampled to determine pore-water composition. At each site, an additional core was collected for mineralogical and geochemical characterization. Total extractable carbonate was measured using the method of Barker and Chatten (1982), and total S was determined using a LECO induction furnace. Samples of the tailings solids were analyzed for total metal concentrations using HF/HNO_3 extraction followed by inductively coupled plasma–optical emission spectrometry (ICP–OES) analysis. Physical properties of the tailings were determined through measurements of grain-size distribution, bulk density, particle density, and volumetric moisture content. The particle density was measured with an air comparison pycnometer, Beckman model 930. The porosity was calculated from the measured bulk density and particle density.

Tailings samples for mineralogical examination were dried at room temperature. Portions of the dried sample were selected for polished thin sections, which were prepared by Vancouver Petrographics Ltd. without the use of water, thereby minimizing the dissolution of readily soluble minerals. The polished thin sections were examined by optical microscopy, using both transmitted and reflected light. Areas of the optical sections were examined further by scanning electron microscopy (SEM) and electron-microprobe analyses. The SEM study utilized a Phillips XL-30 instrument with a coupled energy-dispersion analyzer, located at the University of British Columbia (UBC). The tailings material was also examined by X-ray diffractometry (XRD) using a Siemens rotating-anode instrument at UBC.

3.3. Tailings pore-water sampling

Pore water from the vadose zone was sampled using a squeezing technique. Pore water from cores S3 and S2 was squeezed in the field. All remaining cores were immediately frozen after collection and were shipped to the University of Waterloo, where the core sections

were thawed prior to extraction. The squeezing technique, as described by Patterson et al. (1978), and as later modified by Smyth (1981) and Blowes et al. (1991), involved adding a viscous immiscible liquid (Paraplex) to the top of each core, then applying pressure with a sealed plunger to displace the Paraplex and pore water down through the core. The resulting water samples were collected in 60 mL syringes and passed through 0.45 μm cellulose-nitrate filters. This squeezing technique minimizes the contact between pore-water samples and atmospheric O_2, limiting oxidation during sample collection. Determinations of pore-water Eh and pH were made at least 3 times during the collection of each unfiltered sample to obtain representative results. The Eh was measured using an Orion Pt redox electrode (model 96-78BN), calibrated in Zobell's solution (Nordstrom, 1977) and Light's solution (Light, 1972). The pH was measured using an Orion Ross combination electrode (model 815600) calibrated with standard buffer solutions at pH 7, 4, and 1. Measurements of alkalinity were made on filtered samples using a Hach digital titrator and bromcresol green/methyl red indicator and with 0.16 N H_2SO_4. One aliquot of water was acidified with 12 N trace-metal grade HCl to a pH of <1 for cation analysis, and another aliquot was left unacidified to use for anion analysis. All samples were immediately refrigerated until analysis.

3.4. Groundwater sampling

Pore water from the saturated zone was collected from the piezometers by using a peristaltic pump and polyethylene tubing. All piezometers were bailed dry and allowed to recover prior to sampling. Measurements of Eh and pH were made in a sealed flow-through cell, maintained at groundwater temperature (~8–10 °C). Calibration of the Eh and pH probes was checked before and after each sampling point. Temperature and alkalinity were measured at each location. Samples were filtered with cellulose-nitrate filters and split into two aliquots for anion and cation analysis. All samples were refrigerated until they were analyzed following the same methods as for samples collected from the vadose zone. ^3H in samples collected from the piezometers in nests S1, S14, S2, S3, and S4 was analyzed in the Environmental Isotope Laboratory at the University of Waterloo. The analytical results are reported as ^3H Units (TU). Dissolved H_2S was determined on 50 mL filtered aliquots using the methylene blue procedure (Standard Methods for the Examination of Water and Wastewater, 1992). Samples for CH_4 analysis were unfiltered, not acidified, and were collected in 50 mL glass serum bottles sealed headspace-free using Teflon-lined septa. The CH_4 samples were shipped on ice and analyzed within 72 h by a gas chromatograph equipped with a flame-ionization detector.

3.5. Water chemistry

Samples collected in the field and laboratory to determine cation and anion concentrations were analyzed by the National Laboratory for Environmental Testing, Environment Canada, Burlington, Ontario. Analyses for Al, As, B, Ba, Be, Ca, Cd, Co, Cr, Cu, Fe, K, Mg, Mn, Mo, Na, Ni, Pb, Si, Sr, V, and Zn were by ICP–OES. Concentrations of SO_4 were determined using an automatic colorimetric procedure or ion chromatography. Quality control and accuracy were evaluated by analyzing several standards covering a range of concentration, by analysis of field replicates and splits, and by addition of standards to unknown samples to assess for matrix effects.

3.6. Geochemical modeling

Groundwater chemistry was interpreted with the assistance of the equilibrium/mass-transfer model MINTEQA2 (Allison et al., 1990). The database of MINTEQA2 was modified to make it consistent with that of WATEQ4F (Ball and Nordstrom, 1991). MINTEQA2, which was used to calculate the saturation indices for discrete minerals, allows oxidation–reduction potentials (ORP) either to be entered as measured Eh or to be calculated from a measured oxidation–reduction couple. In acid mine waters, high activities of both Fe(II) and Fe(III) provide a dominant and reversible couple responsive to Pt Eh electrodes (Nordstrom et al., 1979). Pore water from the Camp tailings contains high concentrations of dissolved Fe(II) and Fe(III); therefore, Eh values were entered directly into MINTEQA2 for speciation of Fe in the model calculations.

4. Results and discussion

4.1. Hydrogeology

At the time of sampling, the depth of the water-table in the Camp tailings was 5.7 m below the tailings surface at S4, and intersected the tailings adjacent to Camp Lake (Fig. 2). Groundwater flow is directed downward from the NW and slopes gradually to the edges of the impoundment (Fig. 2). The average hydraulic head measured at piezometer nest S4 was 0.5 m higher than the head measured at S1. The bearing of the groundwater gradient in the Camp tailings during the study period ranged from 284 to 279° (average 281°), and the overall magnitude was 0.004 as calculated using matrix-solving functions in a program formulated by Devlin (2003) (Fig. 3).

The hydraulic conductivity (K), measured from 13 piezometers, ranges from 4.7×10^{-6} to 1.10×10^{-7} $m\,s^{-1}$, with an arithmetic average of 1.5×10^{-6} $m\,s^{-1}$.

The average calculated porosity of the tailings was 0.44. Grain-size distributions were measured on 22 samples extracted from various depths throughout the Camp impoundment. The average d_{10} (mm) of the Camp tailings, which is the grain-size diameter at which 10% by weight of the particles are finer, ranges from 0.04 to 0.1 mm. Hydraulic conductivities of the tailings were estimated using methods developed by Slichter, and Beyer. Methods by Slichter and Beyer are ideal for sediments with a d_{10} ranging from 0.01 mm $< d_{10} <$ 5 mm to 0.06 mm $< d_{10} <$ 0.6 mm, respectively (Vukovic and Soro, 1992). The arithmetic average K calculated from the grain-size analysis was 8.3×10^{-6} m s^{-1} (using the method of Slichter) and 2.7×10^{-6} m s^{-1} (using the method of Beyer), somewhat higher than values obtained from rising-head tests. Recharge for the Camp tailings, calculated using the Dupuit–Forchheimer equation (Freeze and Cherry, 1979) with $K = 8.3 \times 10^{-6}$ m s^{-1} (method of Slichter) was estimated to be 108 mm a^{-1}, which accounts for 22% of the annual precipitation (478 mm a^{-1}).

Atmospherically derived ^{3}H was used to determine the groundwater velocity across the Camp tailings. ^{3}H is used as a tracer in hydrologic studies (Plummer et al., 1993) to determine groundwater velocities for travel times greater than 40 a (Robertson and Cherry, 1989). ^{3}H values measured in piezometers from the Camp tailings range from <6 to 122 TU. ^{3}H concentrations increase along the groundwater flowpath from S4 to S1 (Fig. 4). At S1 adjacent to Camp Lake, ^{3}H ranges from 6 to 122 TU. The highest TU values at S1 occur at a depth of 3.8 m (122 TU) and 5.8 m (121 TU), indicating that this water infiltrated during the peak of atmospheric nuclear testing between 1962 and 1964. Groundwater concentrations of SO_4, Fe, and other metals are elevated across the tailings, including areas of high ^{3}H concentrations, suggesting that meteoric precipitation has displaced AMD water downward and across the tailings into Camp Lake (Fig. 4).

The groundwater velocity, determined with the Darcy equation, water-table gradient, and average porosity and grain-size analysis by using average K values calculated from the methods of Slichter and of Beyer, was 7 and 2 m a^{-1}, respectively. These calculations assume that the mine road to the north is an impermeable boundary and that the groundwater flowpath begins at the edge of the impoundment near S4, extending across the tailings to Camp Lake. Groundwater velocity derived from the ^{3}H data was calculated from the distance peak ^{3}H concentrations traveled along the groundwater flowpath since infiltration in the mid 1960s. The groundwater velocity calculated from the ^{3}H data ranges between 1.7 and 3.4 m a^{-1}, within range of the velocity calculated using the grain-size analysis. Results from the ^{3}H groundwater velocities suggest that the travel time for one pore volume of meteoric precipitation to discharge through the Camp tailings from S4 to S1 is 40 a.

The groundwater velocity was calculated to be 0.7 m a^{-1} from the piezometer-response tests using the method of Hvorslev, an order of magnitude less than the ^{3}H and grain-size values. Several factors may contribute to the discrepancy between the ^{3}H velocity and piezometer-response test. Piezometers installed into the tailings were wrapped with a mesh of stainless steel to protect the Geotextile and NYTEX screen filters. As the piezometer was being driven through the tailings with a vibrating hammer, fine particles within the tailings may have accumulated and packed around and within the steel mesh, reducing the measured K of the surrounding media.

The hydraulic conductivity of the lake sediments underlying the Camp tailings from piezometer nest S2 to S1 ranges between 3.1×10^{-10} and 8.8×10^{-11} m s^{-1} calculated from the piezometer rising-head response-test method of Hvorslev (1951). Vertical hydraulic gradients within the lake sediments are upward, with the greatest gradient observed at piezometer nest S1.

4.2. Sulfide oxidation

The primary non-sulfide gangue assemblage of the Camp tailings consists mainly of quartz, K-feldspar, albite, and biotite. Other primary minerals, mostly in accessory amounts (1–2%) are chlorite and amphibole. Trace amounts of talc [$Mg_3Si_4O_{10}(OH)_2$], ilmenite [$FeTiO_3$], magnesite [$MgCO_3$], sillimanite [Al_2SiO_5], rutile [TiO_2], titanite [$CaTiSiO_5$], gahnite [$ZnAl_2O_4$], and garnet [$Fe_3^{2+}Al_2(SiO_4)_3$], with a few occurrences of cordierite [$Mg_2Al_4Si_5O_{18}$], epidote [$Ca_2Al_2(Fe^{3+}, Al)Si_3O_{12}(OH)$], siderite [$FeCO_3$], clinopyroxene [(Ca,Na)(Mg, Fe,Al)(Si,Al)$_2O_6$], and hematite [Fe_2O_3] were observed in the tailings.

The Camp tailings consist of up to 60 wt% sulfide minerals, principally pyrrhotite and pyrite. Mineralogical examination of the tailings indicates that the ratio of pyrrhotite:pyrite is 1:1 to 2:1, with pyrrhotite equaling or exceeding pyrite in all samples. Other primary sulfide minerals in the tailings are sphalerite, chalcopyrite, marcasite [FeS_2], and trace amounts of arsenopyrite. The oxidation of pyrrhotite and pyrite by atmospheric O_2 can be represented as:

$$\underset{\text{pyrrhotite}}{Fe_{(1-x)}S} + (2 - \frac{1}{2}x)O_2 + xH_2O \Rightarrow (1-x)Fe^{2+} + SO_4^{2-} + 2xH^+ \quad (1)$$

$$\underset{\text{pyrite}}{FeS_2} + \frac{7}{2}O_2 + H_2O \Rightarrow Fe^{2+} + 2SO_4^{2-} + 2H^+ \quad (2)$$

The Fe(II) shown in reactions (1) and (2) can be further oxidized to form Fe(III), which under mildly acidic to

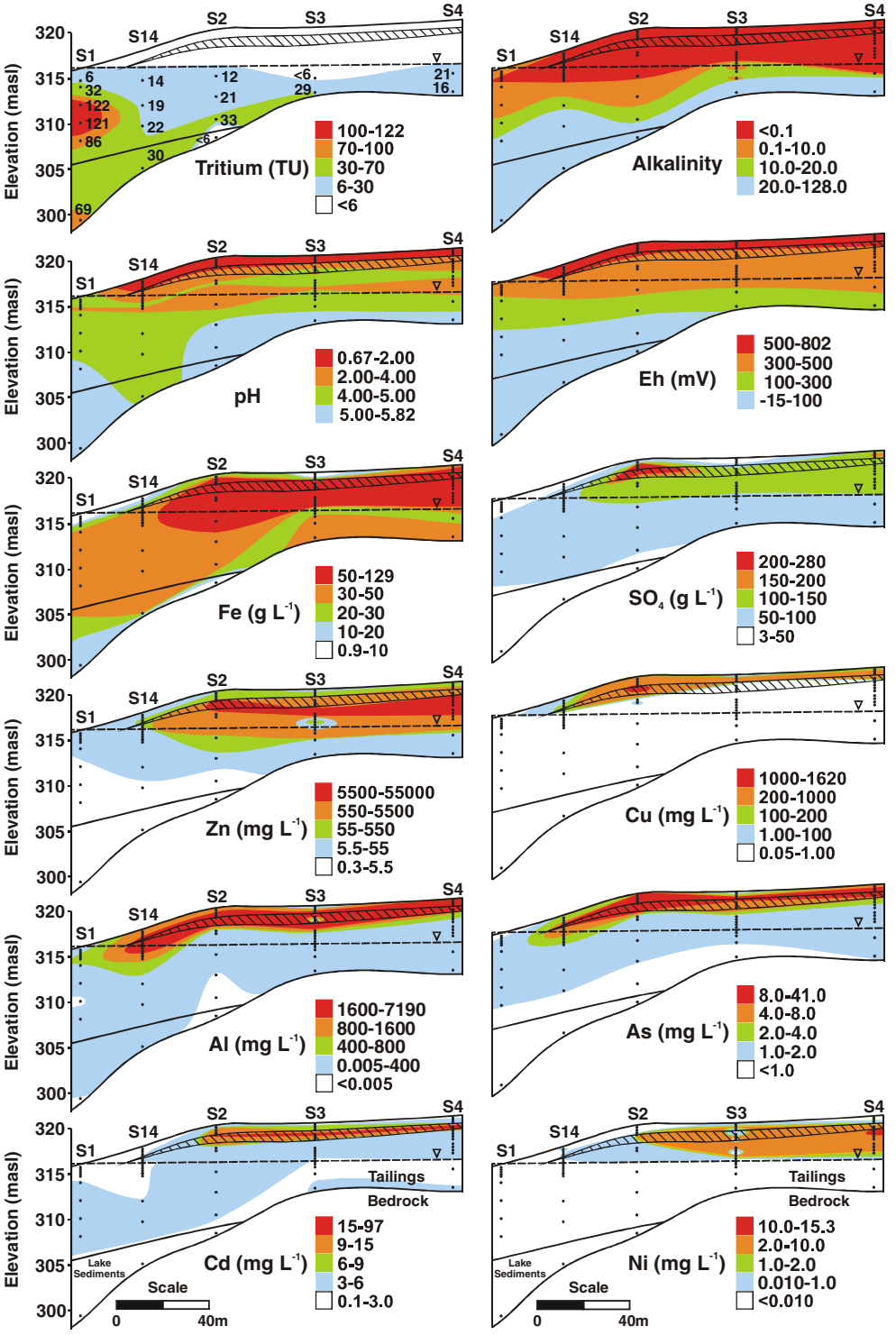

Fig. 4. Water chemistry across the Camp tailings, from S1 to S4, measured in August 2001. Black dots represent piezometer sampling locations. Dashed line with inverted triangle represents the water table. The cross-hatched area indicates the extent of the hardpan. Alkalinity is expressed as mg L^{-1} $CaCO_3$.

near-neutral pH conditions, will precipitate as Fe^{3+} oxyhydroxide as represented by the reaction:

$$Fe^{2+} + \frac{1}{4}O_2 + \frac{3}{2}H_2O \Rightarrow \underset{\text{geothite}}{\alpha FeOOH} + 2H^+ \quad (3)$$

Under very low pH conditions (pH <3), Fe(III) can remain in solution and react with the sulfide minerals through:

$$Fe_{(1-x)}S + (8-2x)Fe^{3+} + 4H_2O \Rightarrow (9-3x)Fe^{2+} + SO_4^{2-} + 8H^+ \quad (4)$$

$$FeS_2 + 14Fe^{3+} + 8H_2O \Rightarrow 15Fe^{2+} + 2SO_4^{2-} + 16H^+ \quad (5)$$

In this case, Fe(II) becomes the dominant form of Fe in solution. Reactions (4) and (5) indicate that for every mole of $Fe_{(1-x)}$ S and FeS_2 oxidized by Fe(III), 8 and 16 moles of H^+ are generated, respectively. The primary mechanisms for sulfide oxidation at pH conditions <3 involves Fe^{3+} as the main oxidant (Nordstrom, 1982). A detailed description of sulfide oxidation reactions is given by Blowes et al. (2003b).

Oxidation reactions in the Camp tailings over the past 70 a have resulted in extensive depletion of sulfide minerals in the near-surface zone of the tailings. Using microscopic analysis, the degree of sulfide alteration intensity (SAI) (Blowes and Jambor, 1990) of the tailings is classified on a scale of 1–10 as described in Table 1. Vertical profiles of SAI, gas-phase O_2, wt% S and $CaCO_3$, and the volumetric moisture content for piezometer nest S3 are shown in Fig. 5. Pore-gas O_2 concentrations decrease from atmospheric concentrations of 20.9% to less than 0.9% in the upper 50 cm of the tailings. An abrupt increase in the abundance of total S, mainly as sulfide minerals, from 9 to 25 wt% S and a decrease in SAI at 50 cm coincide closely with the rapid depletion of pore-gas O_2, which is a consequence of O_2 consumption in accordance with reactions (1) and (2).

Core extracted from piezometer nest S3 is oxidized visibly to a depth of 90 cm, varying in color from rusty-red at the surface of the tailings to a mustard yellow at 90 cm below ground surface. At a depth of 90 cm, a black massive hardpan layer is present. Extensive oxidation has occurred in the upper 30 cm of the tailings, with near-obliteration of all sulfide minerals. The princi-

Table 1
Sulfide alteration index (SAI) of tailings from piezometer site S3

Index	Alteration
10	Almost complete oxidation of sulfides; traces of chalcopyrite ± pyrite
9	Only sparse pyrite and chalcopyrite; no pyrrhotite or sphalerite
8	Pyrite and chalcopyrite common, but chalcopyrite proportion higher than normal possibly because of pyrite dissolution; no pyrrhotite or sphalerite
7	Pyrite and chalcopyrite proportions normal; pyrrhotite absent but sparse sphalerite present
6	Pyrrhotite absent but sphalerite common
5	Pyrrhotite represented by marcasite pseudomorphs
4	First appearance of pyrrhotite, but only as remnant cores
3	Cores of pyrrhotite abundant
2	Well-developed cores of pyrrhotite, with narrower alteration rims; replacement by marcasite decreasing, and pseudomorphs are absent
1	Alteration restricted to narrow rims on pyrrhotite

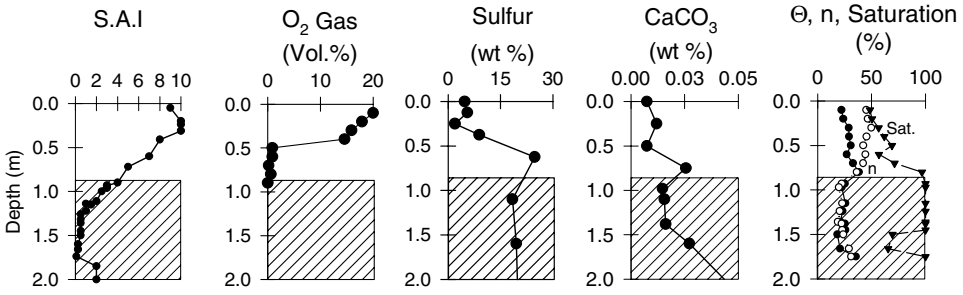

Fig. 5. Depth profiles of the sulfide alteration index (SAI), concentrations of O_2 gas, weight percent of sulfur and carbonate minerals, volumetric moisture content (Θ), porosity (n), and saturation measured at S3. The cross-hatched area represents hardpan. The water table is at a 4.6 m depth.

pal alteration products of sulfide minerals in the oxidized zone of the tailings are goethite, lepidocrocite, jarosite, and native S. At a depth of 40 cm, pyrite and chalcopyrite are unaltered, but sphalerite and pyrrhotite are absent. The first appearance of sphalerite occurs at a depth of 60 cm, but pyrrhotite is absent, suggesting that pyrrhotite is the sulfide mineral most susceptible to replacement in the Camp tailings. Pyrrhotite first appears at the top of the hardpan (90 cm) as remnant cores within pseudomorphs of marcasite (Fig. 6). At a depth of 115 cm, well-developed cores of pyrrhotite are present, and marcasite is restricted to narrow alteration rims. The observed order for decreasing resistance to oxidation of sulfide mineral in the Camp tailings is: chalcopyrite = pyrite>sphalerite>pyrrhotite. The partial alteration to complete pseudomorphism of pyrrhotite is a common feature within the oxidized zone of the tailings; however, the replacement of pyrite is less obvious and is expressed as a depletion rather than as a gradation to residual cores as is the case with pyrrhotite. A few grains of pyrite exhibit black alteration rims consisting of S-bearing epoxy, suggesting that the rims were originally water-soluble Fe sulfates formed locally prior to the development of the Fe^{3+} oxyhydroxide rims that typically characterize the alteration of pyrite (Fig. 7).

Sulfide minerals below the water table do not exhibit alteration, although a significant amount of dissolved H_2S (0.03–0.10 $mg\,L^{-1}$) was observed in tailings water collected from the piezometers. The H_2S can be produced through reaction of acidic waters with pyrrhotite

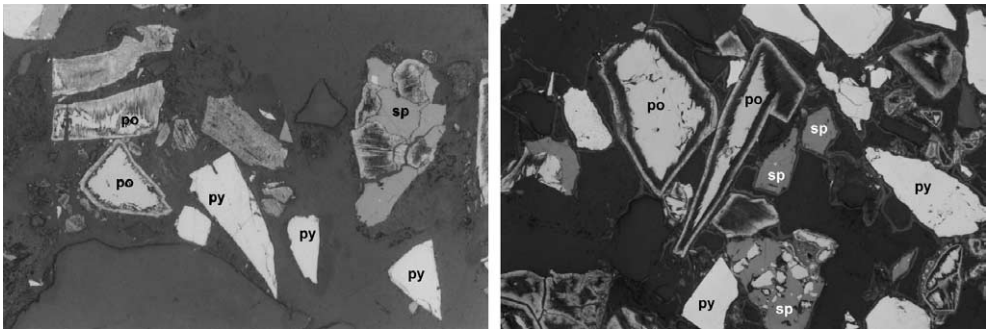

Fig. 6. Photomicrographs in plain reflected light, width of field 0.625 mm; abbreviations are py pyrrhotite, po pyrrhotite, and sp sphalerite. The photo on the left, which is of tailings from 90 cm depth, illustrates various stages toward the pseudomorphism of pyrrhotite; to the left of the largest grain of pyrite is pyrrhotite with a narrow whitish rind of marcasite, and immediately above the rimmed grain is one in which only a residual core of pyrrhotite remains. Above the residual-core grain, and also to its right, are pseudomorphs of marcasite after pyrrhotite. Likewise, the darkish grains intergrown with sphalerite at the far right are marcasite after pyrrhotite, thus illustrating the greater alteration resistance of sphalerite relative to that of pyrrhotite. In the photo on the right, which is of tailings from 110 cm depth, pyrite and sphalerite are unaltered, and near the center are cores of pyrrhotite rimmed by voids (black) that are succeeded by an outermost thin rind of whitish marcasite.

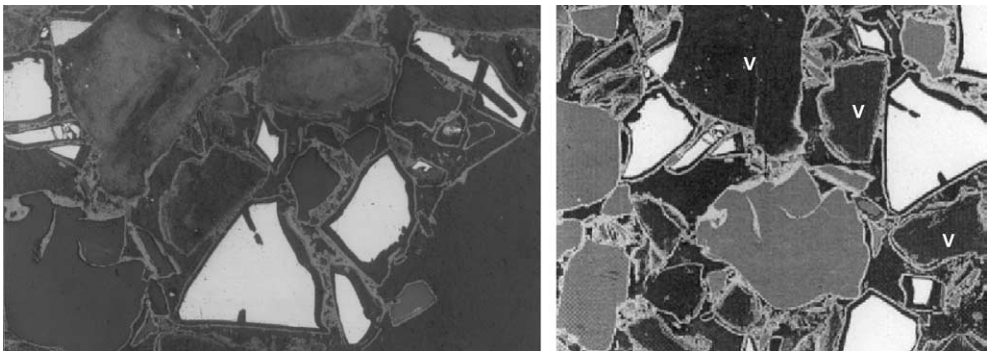

Fig. 7. The photomicrograph to the left shows whitish grains of pyrite and non-sulfide gangue minerals cemented by Fe oxyhydroxide. The black rims on the pyrite grains consist of S-bearing epoxy, suggesting that the rims were originally water-soluble Fe sulphates. The thin outermost rind is Fe oxyhydroxide. Width of field 0.625 mm; sample depth 5 cm at site S3. Part of the same area is shown in the backscattered-electron (BSE) image to the right, wherein the thin rinds around large, blackish particles are interpreted to outline former grains of pyrrhotite (e.g., the three marked with 'v').

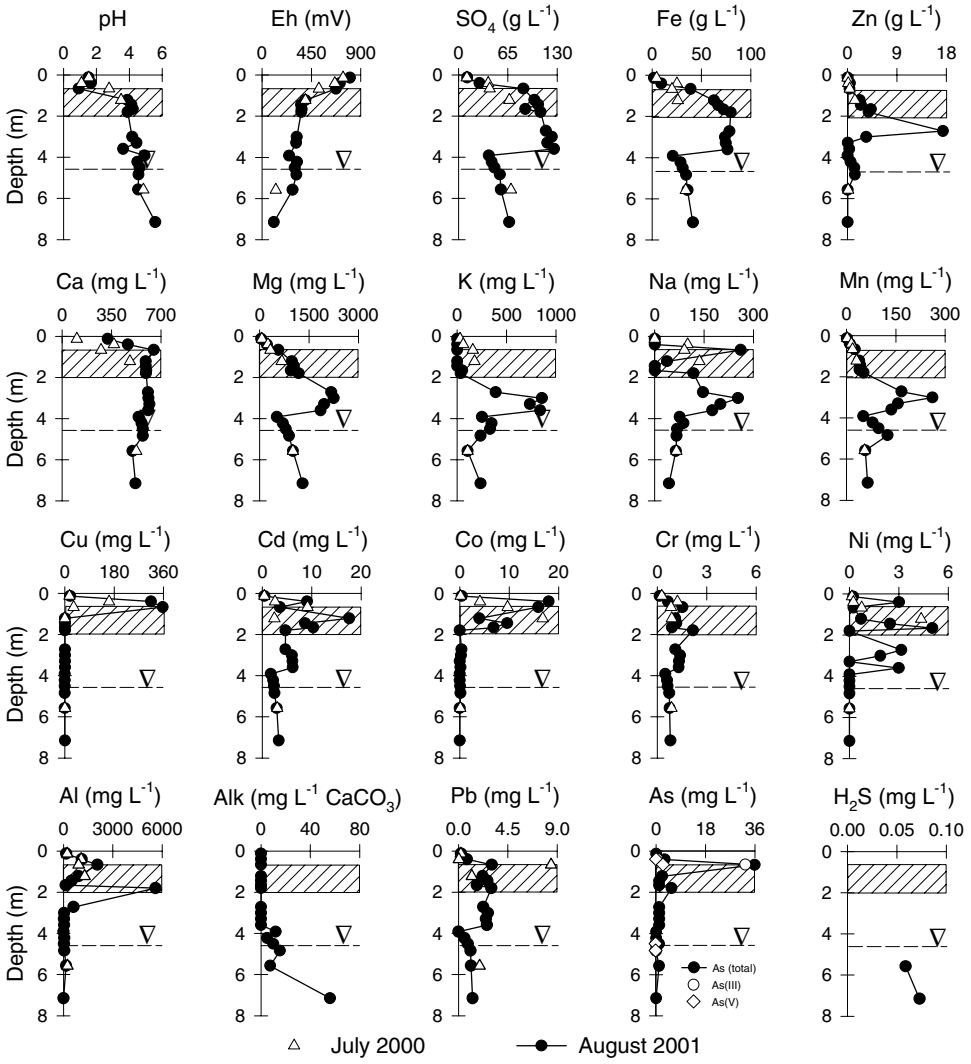

Fig. 8. Water-chemistry profiles for piezometer nest S3. Dashed line with inverted triangle represents the water table. The cross-hatched area indicates the extent of the hardpan.

and sphalerite (Nordstrom and Alpers, 1999). The H_2S could also be produced by bacterially mediated SO_4 reduction reactions (Gould and Kapoor, 2003). Methane concentrations measured in piezometers range from 1.1 to 222 $\mu g L^{-1}$, indicating that methanogenesis may be occurring.

4.3. Pore-water chemistry

Seventy years of sulfide oxidation of the Camp tailings has resulted in the generation of low-pH tailings pore water that contains high concentrations of metals and SO_4. Above the hardpan layer, the pH of the tailings pore water is as low as 0.67, and the Eh ranges from 800 to 680 mV (Fig. 4). The pH increases abruptly where the hardpan is first encountered, gradually increasing with depth. The Eh decreases at the hardpan and continues to decrease with depth. Across the tailings, high concentrations of Fe, SO_4, and most dissolved metals coincide with low pH conditions (<1) at the top of the hardpan and increase with depth through the hardpan to just above the water table (Fig. 8). Extremely high concentrations of Fe (129,000 $mg L^{-1}$), SO_4 (280,000 $mg L^{-1}$), Zn (55,000 $mg L^{-1}$), Al (7200 $mg L^{-1}$), Cd (97 $mg L^{-1}$), Co (110 $mg L^{-1}$), Cu (1600 $mg L^{-1}$), Cr (3 $mg L^{-1}$), Mn (260 $mg L^{-1}$), Ni (15 $mg L^{-1}$), Pb (8 $mg L^{-1}$), and As (40 $mg L^{-1}$) were observed in the vadose zone of the impoundment. Measurable alkalinity was rarely detected at any location in the unsaturated zone. Table 2, which is an updated version of that in Nordstrom and

Table 2
Comparison of some of the most acidic waters and highest concentrations of metals derived from tailings pore water, surface water, and underground mine workings

Parameter ($g L^{-1}$) (except pH)	pH	Cu	Zn	Cd	As	Fe_{total}	SO_4
Sherridon tailings (tailings pore water)[a]	0.67	1.6	55	0.1	0.05	129	280
Heath Steele (tailings pore water)[b]	0.80	0.6	6	n/a	n/a	48	85
Genna Luas (surface water)[c]	0.60	0.22	10.8	0.06	0.07	77	203
Iron Mountain (mine shafts/drifts)[d]	−3.6	4.76	23.5	0.21	0.34	141	760
Other sites (mine shafts/drifts/pore water[i])	0.67[e]	468[f]	50[g]	0.04[h]	22[i]	57[i]	209[h]

[a] Moncur et al. (2003).
[b] Blowes et al. (1991).
[c] Frau (2000).
[d] Nordstrom et al. (2000).
[e] Goleva et al. (1970).
[f] Clarke (1916).
[g] Braeuning (1977).
[h] Lindgren (1928).
[i] Giere et al. (2003).

Alpers (1999), compares some of the most acidic waters and highest concentrations of metals derived from mining environments. Concentrations of dissolved Zn from the Camp tailings are among the highest reported for waters impacted by mining activities.

Directly above the water table, most metals and SO_4 show a sharp decrease in concentration. Below this depth the concentrations are lower, but still remain well above regulatory standards. This concentration front likely represents a peak period of sulfide oxidation reactions during which very high concentrations of oxidation products were released to the vadose zone pore waters. Although dissolved concentrations of metals and SO_4 decrease below the water table, the concentrations remain elevated throughout the impoundment, with Fe and SO_4 values up to 60,600 and 91,600 $mg L^{-1}$, respectively, in the deeper groundwater (Fig. 4). Across the tailings, from piezometer nest S4 to S1, high concentrations of Fe, SO_4, Zn, Al, Cu, Cr, Co, Cd, Pb, Ni, and As were detected in nearly all piezometers. Alkalinity in the groundwater ranges between 0 and 127 $mg L^{-1}$ (as $CaCO_3$), with the highest values observed deep in the impoundment.

The ionic strength of the tailings pore water varies from 0.14 to 12.7, beyond the optimum range of activity corrections calculated with MINTEQA2 using the Extended Debye–Huckel or Davies equations (Blowes et al., 1991; Ptacek and Blowes, 2000). Application of the Pitzer equations using PHRQPITZ (Plummer et al., 1988) allows the determination of activity coefficients for high ionic strength waters. The database of PHRQPITZ was modified to include parameters required to apply the Pitzer equation to mine drainage-waters (Ptacek and Blowes, 2003). In addition, the MINTEQA2 database was modified to include equilibrium constants derived from the WATEQ4F. These equilibrium-constant values were selected to improve predictive modeling for high-Fe and -SO_4 mine waters. Saturation indices of pore water from the Camp tailings were calculated for melanterite and gypsum using PHRQPITZ and MINTEQA2 (Ptacek and Blowes, 2003) (Fig. 9). Both models show similar trends in

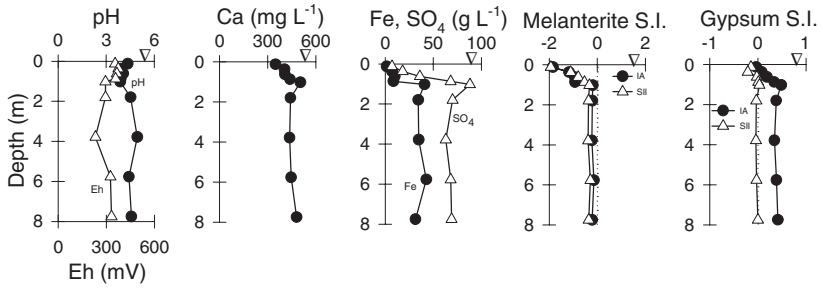

Fig. 9. Saturation indices (SI) for melanterite and gypsum at piezometer nest S1. IA is the ion-association SI calculated using MINTEQA2. SII is the specific ion-interaction SI calculated using PHRQPITZ, after Ptacek et al. (2001).

saturation indices for melanterite. The tailings pore water is undersaturated with respect to melanterite near the surface of the tailings, and then becomes saturated at 1 m depth, where the activities of Fe, SO_4, and Ca increase. Results from PHRQPITZ calculations show that gypsum attains saturation at a 1 m depth, but MINTEQA2 calculations indicate supersaturation. For concentrated solutions, saturation indices for SO_4-bearing minerals calculated with PHRQPITZ have been observed to correspond more closely to expected saturation states (Ptacek and Blowes, 2000). The discrepancy between the saturation index values calculated using the ion-association model adopted by MINTEQA2 and the PHRQPITZ calculation results arises from the application of the extended Debye–Huckel equation beyond the range of accuracy (Blowes et al., 1991; Ptacek, 1992; Ptacek and Blowes, 2000, 2003). This discrepancy is more pronounced for gypsum than melanterite. Equilibrium constants are typically determined from dissolution experiments which dissolve the mineral in pure water. Because the solubility of gypsum is lower than that of melanterite, the gypsum equilibrium constant values are derived from a solution with a lower ionic strength than for melanterite. As a result, the effect of the high ionic strength waters observed at Sherridon is more pronounced on the gypsum SI values than for the melanterite SI values.

4.4. Acid neutralization

The oxidation of sulfide minerals results in the release of H^+ into the tailings pore water. Gangue minerals incorporated in the tailings can neutralize the H^+. Examples of gangue that can contribute appreciably to acid-neutralizing reactions include calcite, dolomite, and aluminosilicate minerals. Their dissolution typically leads to a distinct sequence of pH-buffering plateaus (Blowes and Ptacek, 1994; Jurjovec et al., 2002; Blowes et al., 2003a). At the Camp impoundment, the porewater pH increases in 3 distinct steps separated by plateaus of reasonably uniform pH. These plateaus occur at a pH of 5.6, 4.3, and 1.4, corresponding to the dissolution of carbonates, Al hydroxides, and aluminosilicates, respectively. Similar pH-buffering sequences have been observed at other sulfide tailings impoundments (Dubrovsky et al., 1984; Blowes and Jambor, 1990; Blowes et al., 1991; Coggans et al., 1999; Johnson et al., 2000).

Carbonate minerals in the Camp tailings make up <0.05 wt% in the vadose zone and <1 wt% in cores of the deeper tailings below the water table. Mineralogical analysis indicates that carbonate minerals are absent in the vadose zone of the S3 profile, except at a depth of 91 and 114 cm, where a few grains of primary siderite were observed. Geochemical modeling using MINTEQA2 indicates that the tailings pore water is undersatu-

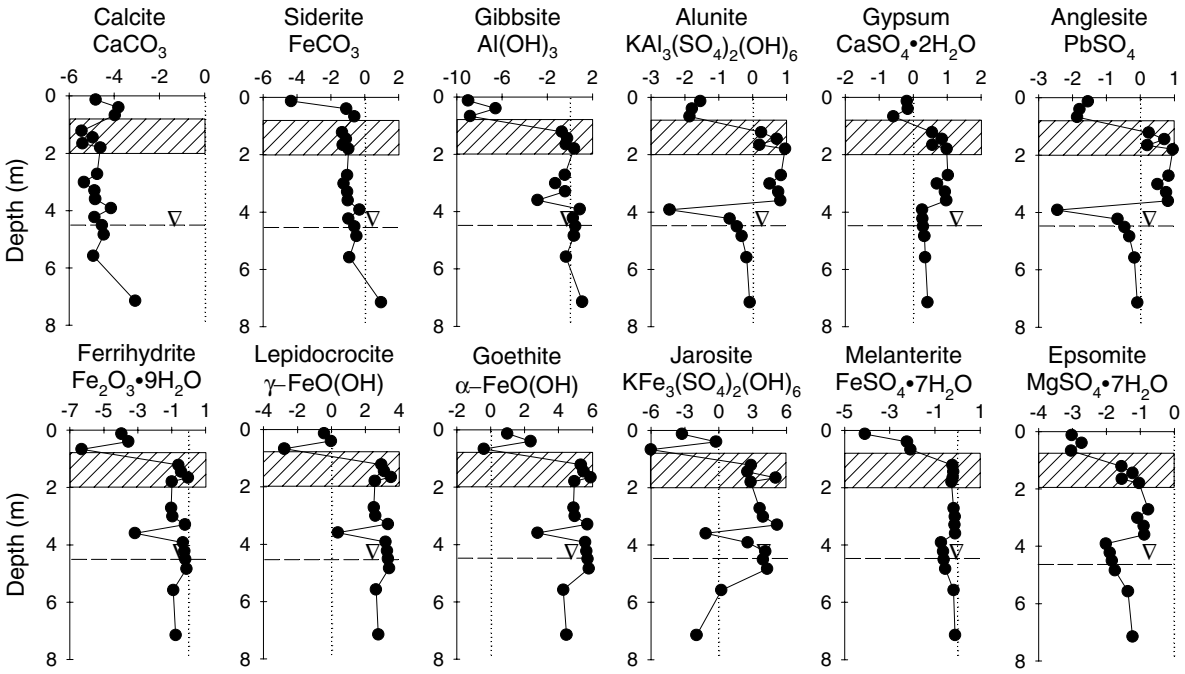

Fig. 10. SI calculated using MINTEQA2, plotted versus depth at piezometer nest S3. Dashed line with inverted triangle represents the water table. The cross-hatched area indicates the extent of hardpan.

rated with respect to calcite [$CaCO_3$] throughout the impoundment (Fig. 10). Calculations using MINTEQA2 also suggest that the tailings water becomes saturated to supersaturated with respect to siderite at a depth of 7.2 m (Fig. 10), consistent with the first observation of alkalinity (Fig. 8). Water samples collected from S1, S2, and S3 at depth have pH values that range from 5.4 to 5.8, and are saturated with respect to siderite, suggesting that siderite dissolution is an important pH-buffering reaction deeper in the tailings.

The second pH plateau ranges from 3.9 to 4.9, from the top of the hardpan extending downward into the water table, and corresponds to pore-water concentrations of Al as high as 4980 mg L^{-1}. The abrupt increase in pH at the depth of the hardpan may be due to the dissolution of a secondary Al mineral. Similar pH ranges, along with elevated concentrations of Al, were observed in $Al(OH)_3$ buffering zones by Dubrovsky et al. (1984), Blowes (1990), Coggans et al. (1999), and Johnson et al. (2000). Calculations using MINTEQA2 indicate that the pore water above the hardpan layer is consistently undersaturated with respect to gibbsite, rapidly becomes saturated near the top of the hardpan, and remains at or near saturation through the vadose zone (Fig. 10). At depth, where the pore water is saturated with respect to siderite, the water becomes supersaturated with respect to gibbsite, and the concentrations of Al decrease to <3.1 mg L^{-1}. These observations suggest that a secondary Al-bearing mineral within and below the hardpan is dissolving. This dissolution, represented as $Al(OH)_3$, can be described through the reaction:

$$Al(OH)_3 + 3H^+ \Longleftrightarrow Al^{3+} + 3H_2O \quad (6)$$

The dissolution of $Al(OH)_3$ consumes 3 moles of H^+; however, the Al^{3+} is released and can reprecipitate in areas of higher pH, releasing H^+.

During the mineralogical study, no secondary $Al(OH)_3$ minerals were identified. This could be because the masses of Al are low and $Al(OH)_3$ precipitates are difficult to identify, or because other Al-bearing minerals are present (Blowes et al., 2003a). Despite the overwhelming predominance of Fe in the system at Sherridon, minor amounts of secondary alunite [$KAl_3(SO_4)_2(OH)_6$] were observed to coexist with secondary SO_4 rims that occur at the margins of pyrrhotite grains in the hardpan. Speciation modeling indicates that the pore water becomes saturated or supersaturated with respect to alunite within the hardpan layer (Fig. 10). Aluminum was also detected by EDS analyses to be present in jarosite and in amounts up to 9 wt% in association with Fe-oxyhydroxide minerals compositionally corresponding to [(Fe,Al)OOH].

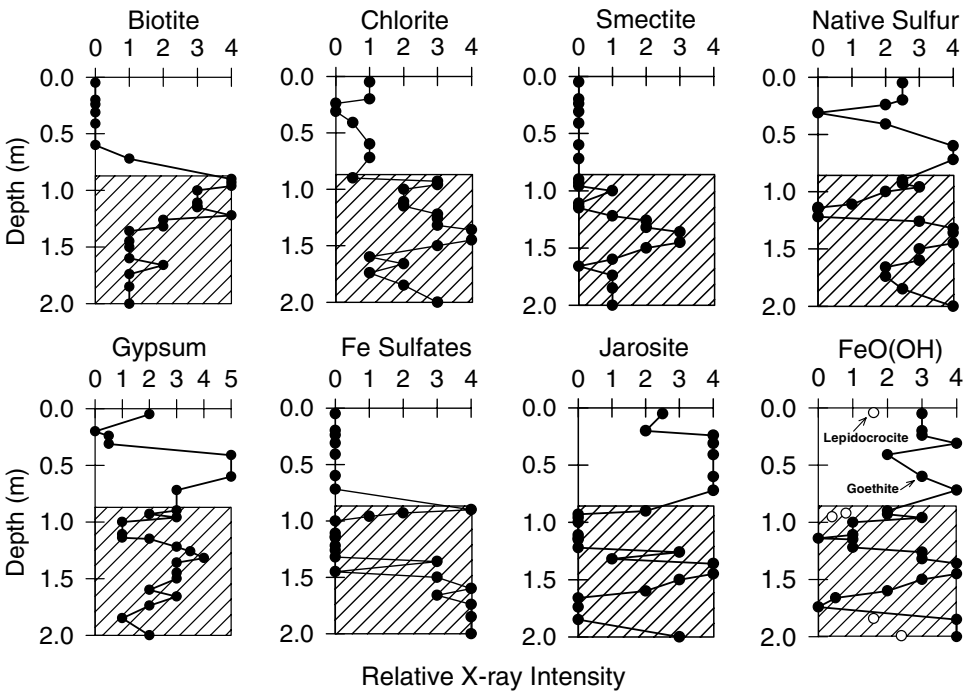

Fig. 11. Mineral distribution versus depth at S3. In the plot for FeO(OH), the solid circles are for goethite and the open circles are for lepidocrocite. Scale on the *x* axis corresponds to the abundance of the mineral on a sample-to-sample comparison of the peak height of a specific X-ray reflection where: 0 – no detection; 1 – very weak detection; 2 – weak detection; 3 – moderate detection; 4 – strong detection; 5 – very strong detection. The cross-hatched area represents hardpan; the water table is at 4.6 m depth.

Gangue minerals contributing to acid-neutralization reactions are predominantly aluminosilicates, among which are biotite and lesser amounts of chlorite. Fig. 11 represents the vertical variation in the distribution of aluminosilicate minerals and secondary precipitates determined using X-ray diffractometry. The scale in Fig. 11 is based on the abundance of the mineral on a sample-to-sample comparison of the peak height of a specific X-ray reflection, such as (0 0 1) for biotite and (0 0 2) for chlorite; therefore, the scale is relative, and no percentages are implied.

The extremely low pH of the pore water (pH 0.67–2) in the upper 90 cm of the tailings has depleted nearly all biotite, chlorite, and smectite to the top of the hardpan layer. The derivation of dissolved Al and K in the pore water of the tailings is from the dissolution of aluminosilicates. When pH values are near neutral, such as during the earliest stages of sulfide oxidation, incongruent dissolution of biotite (Kalinowski and Schweda, 1996; Malmström et al., 1996) may result in vermiculitization of the biotite (Banfield and Eggelton, 1988; Murakami et al., 2003):

$$K(Mg_2Fe)(AlSi_3)O_{10}(OH)_2 + 5H^+ + 0.25O_2 + 3H_2O \Rightarrow 0.5Al_2Si_2O_5(OH)_4 + Fe(OH)_3 + 2H_4SiO_4 + K^+ + 2Mg^{2+} \quad (7)$$

The alteration of one mole of biotite to vermiculite and thence to kaolmite, as in reaction (7), results in the consumption of 5 moles of H^+, precipitation of Fe oxyhydroxide, and release of K^+ and Mg^{2+} to the pore waters. The first ions released during the dissolution of biotite are alkali and alkaline-earth cations (Rufe and Hochella, 1999) where K^+ may precipitate from solution as jarosite, releasing 6 moles of acid:

$$K^+ + 3Fe^{3+} + 2SO_4^{2-} + 6H_2O \Longleftrightarrow KFe_3(SO_4)_2(OH)_6 + 6H^+ \quad (8)$$

The precipitation of jarosite is a commonly observed reaction in oxidized tailings impoundments (Jambor, 1994). Jarosite forms mainly in acidic environments (Barker et al., 1998) and was observed throughout the oxidation zone of the tailings. XRD analysis indicates a moderate to very strong detection of the secondary minerals jarosite, goethite, lepidocrocite, and gypsum in the upper 90 cm of the tailings (Fig. 11). Geochemical modeling of the tailings pore water also indicates that this water approaches or becomes saturated with respect to jarosite, goethite, lepidocrocite, and gypsum in areas within the upper 90 cm of the tailings.

Only traces of hydrobiotite, which is a 1:1 interlayer of biotite and vermiculite, were identified in the low-pH zone where biotite is depleted. In the biotite-depleted areas, silica pseudomorphs after biotite were observed to contain little Mg^{2+} or Al^{3+} (<0.5 wt% of each as oxides), and are interpreted to be silica remnants after leaching of the original Mg–Fe–Al content (Fig. 12). An increase in H^+ ion activity in the pore water through reactions (1), (2), (3), (4), (5) and (8) will increase the dissolution rate of biotite (Kalinowski and Schweda, 1996), consuming the acid-neutralization potential. At a pH below 3.1, biotite will dissolve congruently and secondary minerals should not precipitate (Taylor et al., 2000). The congruent dissolution of biotite, using the stoichiometry observed for the mineral in the Camp tailings, leads to the following reaction:

$$K_{0.95}(Mg_{1.76}Al_{0.44}Fe_{0.61})Al_{1.26}Si_{2.74}O_{10}(OH)_2 + 11.4H^+ + 0.09O_2 \Rightarrow 0.95K^+ + 1.76Mg^{2+} + 0.61Fe^{3+} + 1.7Al^{3+} + 2.74H_4SiO_4 + 1.22H_2O \quad (9)$$

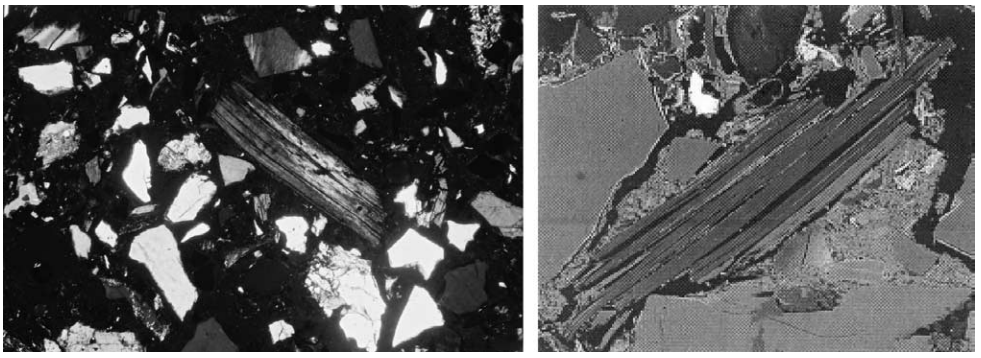

Fig. 12. On the left is a photomicrograph of tailings from 41 cm depth, site S3; transmitted light, crossed polarizers, width of field 2.6 mm. The photo shows at the center a large lath of former biotite, still with good cleavage traces but now a pseudomorph consisting of amorphous hydrous silica. The photo on the right is a BSE image of similarly replaced biotite, but with an unreplaced remnant evident as the lighter grey lath-like portion at the bottom right. Site S3, depth 5 cm, width of image 0.325 mm.

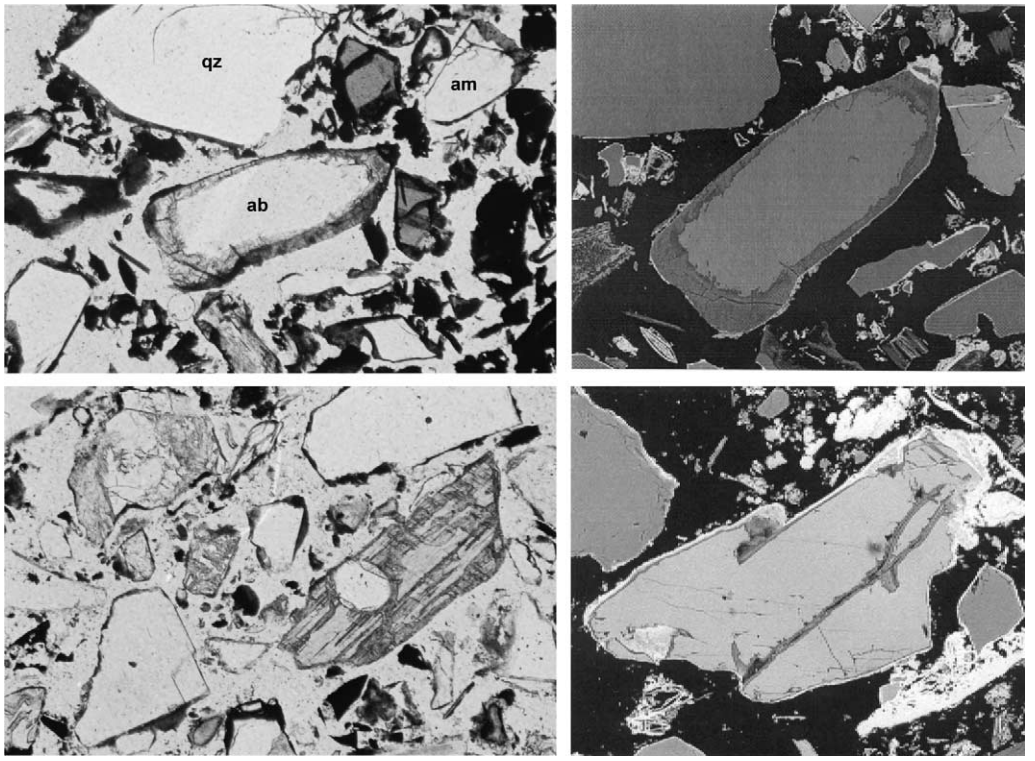

Fig. 13. Upper left photomicrograph in plain transmitted light shows the partial replacement of albite by amorphous hydrous silica that forms a complete rim; width of field 1.2 mm; albite (ab), quartz (qz), amphibole (am). To the right is the corresponding BSE image. The whitish exterior film is Fe oxyhydroxide. The lower left photomicrograph in plain transmitted light, width of field 0.625 mm, shows an oval grain of quartz within amphibole that is extensively replaced by silica. At the lower right is a BSE image showing an amphibole grain that is veined and rimmed by (darker) amorphous hydrous silica. The outermost rind and nearby white particles are Fe oxyhydroxides; width of field 350 μm.

The dissolution of 1 mol of biotite consumes 11.4 moles of H^+, releasing Mg^{2+}, Fe^{3+} and Al^{3+} into the pore water. As sulfide oxidation and acid generation continue, products from the initial incongruent-dissolution reactions (Fe oxyhydroxides and Fe hydroxysulfates) may dissolve, resulting in additional acid neutralization (Blowes, 1990). Above the hardpan there is also evidence that the more stable aluminosilicates have been susceptible to replacement, thereby contributing to acid neutralization. Grains of albite [$(Na_{0.65}Ca_{0.34}K_{0.01})_{\Sigma 1.00}(Si_{2.64}Al_{1.37})_{\Sigma 4.01}O_8$], cordierite [$(Mg_{2.07}Fe_{0.07}Na_{0.06}Mn_{0.02})_{\Sigma 2.22}Al_{4.00}(Si_{4.74}Al_{0.23})_{\Sigma 4.97}O_{18}$], and amphibole [$(Na_{0.48}Ca_{0.15}K_{0.06})_{\Sigma 0.69}(Ca_{1.58}Fe_{0.39}Mn_{0.03})_{\Sigma 2.00}(Mg_{2.51}Fe_{1.73}Al_{0.63}Ti_{0.13})_{\Sigma 5.00}(Si_{6.33}Al_{1.67})_{\Sigma 8.00}O_{22.93}F_{0.07}$] exhibit rims and veinlets of secondary silica that have partly replaced the minerals (Fig. 13). The dissolution of albite, cordierite and amphibole releases additional Al, K, Fe, and Mg, along with Ca, Na, and Mn, to the pore water. The depletion of aluminosilicate minerals in the upper meter of the tailings, and the presence of a significant amount of residual sulfide minerals in this zone after 70 a of oxidation, suggest that the zone of low-pH pore water will likely expand as sulfide oxidation and acid generation continue.

4.5. Hardpans

The Camp tailings have two distinct types of hardpans. A massive (>1 m thick) hardpan that is present throughout the impoundment ranges in depth from 0.5 to 2 m below ground surface and is mainly cemented by Fe^{2+} minerals. Above this ferrous iron hardpan are thin (1–10 cm), discontinuous hardpan layers composed of Fe^{3+}-bearing minerals.

4.5.1. The ferrous iron hardpan

A blackish ferrous hardpan is present throughout the impoundment, but pinches out at the edges adjacent to water bodies and zones of groundwater discharge. At piezometer nest S3, the hardpan is 40 cm below the zone of active oxidation and is 1 m thick. The surface is strongly cemented and is difficult to penetrate even with a backhoe. During pit excavations to penetrate

the hardpan in July 2000, layers of fibrous melanterite [$FeSO_4 \cdot 7H_2O$] up to 1 cm thick were observed along the surface of the hardpan. The melanterite was also observed to have crystallized in situ along vertical fractures and horizontal bedding planes in the upper 15 cm of the hardpan. Energy-dispersion and XRD analysis of the melanterite indicated it to be almost pure $FeSO_4 \cdot 7H_2O$ with only a trace amount of Cu (<0.25 wt%) and with Zn, Mg, and Mn below detection limits. During pit excavations a year later (July, 2001), encrustations of melanterite were not encountered along the surface of the hardpan. Precipitation records show that there was a greater amount of rainfall prior to sampling in 2001 than in 2000. The formation of melanterite may temporarily retard the release of Fe(II), SO_4, and indirectly H^+, to the pore water; however, melanterite is highly soluble and can be rapidly dissolved by rainwater (Jambor et al., 2000; Frau, 2000), which could explain the absence of the mineral during the 2001 pit excavation.

Mineralogical examination of hardpan samples indicates that the principal components of the pore-filling cements are Fe^{2+} minerals, including melanterite and rozenite, and lesser amounts of the Fe^{3+} -bearing minerals such as jarosite, goethite, lepidocrocite, and ferrihydrite (Fig. 11). Gypsum was also observed as a major cement-forming secondary mineral within the hardpan. Blowes et al. (1991) encountered a similar hardpan layer at the Heath Steele mine in New Brunswick, Canada, where the predominant cementing minerals were melanterite and gypsum. MINTEQA2 and PHRQPITZ calculations indicate that the pore water in the Camp tailings at the top of the hardpan attains saturation with respect to melanterite and is supersaturated with respect to gypsum, jarosite, goethite, and lepidocrocite, consistent with the mineralogical observations. The precipitation of Fe^{2+} sulfates, gypsum, jarosite, and Fe oxyhydroxides limits the pore-water SO_4, Fe, and Ca concentrations. The high sulfide content in the Camp tailings consumes atmospheric O_2 near the tailings surface, and reduces Fe(III) to Fe(II) deeper in the tailings. This reaction results in lower concentrations of Fe(III), whereas concentrations of Fe(II) and SO_4 are sufficient to attain saturation with respect to Fe^{2+} SO_4 minerals below the zone of oxidation (Blowes et al., 1991).

High moisture contents were observed above the hardpan at S3. The moisture content increases from the tailings surface to the top of the massive hardpan, and then sharply decreases within the hardpan layer (Fig. 5). The porosity of the tailings decreases from 0.45 at the surface of the tailings to 0.36 at the top of the hardpan, then abruptly decreases to an average of 0.23 within the hardpan layer (Fig. 5). The decrease in porosity within the hardpan is due to the precipitation of secondary minerals, which infill pore spaces. Saturation of the tailings is 50% at the surface, increases with depth, and becomes 100% within the upper 0.5 m of the hardpan. The results in Fig. 5 suggest that the low permeability of the hardpan limits the amount of recharge, causing water to pool above the hardpan and creating a perched water table. The permanent water table is 4.6 m below the surface near S3. The flow of groundwater derived from the vadose zone can be due either to a transient rise in the water table during storm events (Blowes and Gillham, 1988; Al and Blowes, 1996) or to perched water-table conditions. The water table at S3 was not observed to fluctuate more that 0.7 m during the study period from July 2000 to June 2002. It is hypothesized that an important transport pathway of metals to the surface-water flow system at the Camp tailings is the result of groundwater flow along the surface of the hardpan layer. This flow is constrained by the contrast in hydraulic characteristics between the hardpan layer and the overlying tailings. During some of the pit excavations through the hardpan layer, the tailings directly above the hardpan appeared to be more saturated than the overlying tailings, and in one case the water oozed from the pit walls above the hardpan immediately after a rain event.

During rainfall events, surface seeps develop along the flanks of the tailings impoundment. Pore water with a geochemical composition similar to that of water directly above and within the hardpan discharges at these seepage zones. Seepage water is greenish and contains high concentrations of Fe (67,800 $mg\,L^{-1}$), SO_4 (151,000 $mg\,L^{-1}$), Zn (164 $mg\,L^{-1}$), Al (1130 $mg\,L^{-1}$), Cd (3.9 $mg\,L^{-1}$), Mn (103 $mg\,L^{-1}$), Pb (1.7 $mg\,L^{-1}$), As (1.8 $mg\,L^{-1}$) and a pH of 3.20. Along the fringes of the seepage zones during late fall and early spring, when temperatures are low, accumulation of melanterite was observed. Geochemical modeling of the seepage water indicates that it is saturated with respect to melanterite (SI = 0.074). The formation of melanterite and the color of the seepage water suggest that most of the Fe in the pore water is Fe(II). The low pH of the seepage water may slow the oxidation of Fe(II) and limit accumulation of Fe^{3+}-bearing minerals. No evidence of Fe^{3+} precipitates is observed along the flowpath of the seepage water until the water discharges into surface water bodies, where massive accumulations of Fe^{3+} minerals are present. During the summer months, when temperatures are higher, melanterite is not observed at the seepage zones; however, a whitish gray powdery precipitate blanketed the seepage area. Mineralogical analysis was not conducted on the whitish gray mineral, but it is likely rozenite [$FeSO_4 \cdot 4H_2O$], possibly with associated szomolnokite [$FeSO_4 \cdot H_2O$]. With increasing temperature or decreasing water activity, melanterite typically dehydrates to rozenite (Jambor and Traill, 1963; Alpers et al., 1994; Chou et al., 2002). These results suggest that shallow lateral flow related to a transient, perched water table

is resulting in the discharge of high concentrations of metals, SO_4, and acid to the tailings surface and adjacent water bodies. Although the Fe^{2+}-bearing hardpan may divert some infiltrating water directly to surface waters, the hardpan does not prevent infiltrating water from penetrating deeper into the tailings, as is evident from the extremely high concentrations of metals and SO_4 in the pore water of the hardpan and underlying water table.

4.5.2. The Fe^{3+}-bearing hardpan

Above the Fe^{2+} hardpan, in the zone of active oxidation, are thin (1–10 cm), discontinuous, yellow–orange to dark red–brown hardpan layers. Mineralogical analysis indicated that the cementing materials of these hardpans are primarily composed of secondary goethite and lepidocrocite, ferrihydrite, jarosite, and gypsum (Hawthorne and Kennedy, 1987; Kamineni and McGregor, 1989). Previous studies of inactive mine-tailings impoundments have reported similar hardpans composed of Fe(III) cementing minerals (e.g., Blowes and Jambor, 1990; Blowes et al., 1991; Tassé et al., 1997; Coggans et al., 1999; Johnson et al., 2000; McGregor and Blowes, 2002; Courtin-Nomade et al., 2003; Giere et al., 2003). At the Camp tailings, the massive Fe^{2+}-bearing hardpan has formed in advance of the oxidation front. The oxidation front is migrating downward over time; therefore, it is likely that the massive Fe^{2+}-bearing hardpan is also moving downward over time. The discontinuous Fe^{3+}-bearing hardpans present in the oxidized zone may be relics of the original Fe^{2+} hardpan.

4.6. Geochemical correlations

The order of abundance of metals in the unoxidized tailings solids, as determined by metal concentrations, is Fe > Al > Zn > Cu > Mn > Co > Pb > Ni > Cr (average concentrations 246 $mg\,g^{-1}$ Fe, 31 $mg\,g^{-1}$Al, 7.7 $mg\,g^{-1}$ Zn, 2.2 $mg\,g^{-1}$ Cu, 0.25 $mg\,g^{-1}$ Mn, 0.08 $mg\,g^{-1}$ Co, 0.07 $mg\,g^{-1}$ Pb, 0.01 $mg\,g^{-1}$ Ni, and 0.005 $mg\,g^{-1}$ Cr). A similar order of abundance was observed in maximum pore-water concentrations measured at piezometer nest S3, except for concentrations of dissolved Zn, which are 3 times greater than those of dissolved Al.

4.6.1. Zinc and Cd

Zinc is released to the pore water by the oxidation of sphalerite $[(Zn_{0.96}Fe_{0.04})_{\Sigma 1.00}S]$. The very high concentrations of Zn are present because sphalerite was not recovered from the ore during the early period of tailings deposition. Calculations with MINTEQA2 indicate that the tailings water is undersaturated with respect to all discrete Zn-bearing secondary minerals included in the database. Mineralogical analysis did not detect any secondary Zn precipitates, but SEM analysis revealed the presence of Zn in all of the Fe oxyhydroxide samples analyzed. The occurrence of Zn with Fe oxyhydroxides suggests that removal of Zn through coprecipitation or adsorption reactions is likely the dominant solid-phase control on the mobility of Zn.

Results from electron-microprobe analyses indicate that sphalerite is the primary source of Cd. Of the 3 sphalerite grains analyzed, the Cd content was well above detection limits. The high concentrations of Cd observed within the tailings pore water are likely due to the abundance of sphalerite in the tailings. Geochemical modeling suggests that the pore water in the tailings is undersaturated with respect to Cd minerals, and secondary Cd precipitates were not encountered during the mineralogical study.

4.6.2. Copper, Pb, and Cr

The oxidation of chalcopyrite is the primary source of dissolved Cu in the tailings pore water. Concentrations of Cu in the tailings pore water reach a maximum of 360 $mg\,L^{-1}$ directly above the hardpan, then rapidly drop to <1.2 $mg\,L^{-1}$ within the hardpan at piezometer nest S3. Mineralogical studies indicate grains of secondary Cu sulfides, predominantly covellite [CuS], first appear within the top of the hardpan and continue to be detected with depth (Fig. 14). Geochemical modeling shows that the pore water is undersaturated with respect to all other Cu-bearing secondary minerals in the MINTEQA2 database. The abrupt decrease in dissolved Cu in the vicinity of the first detection of covellite suggests that the precipitation of secondary Cu–sulfide minerals is controlling Cu concentrations. Covellite was identified as the secondary solid-phase control of dissolved Cu in the Waite Amulet tailings (Blowes and

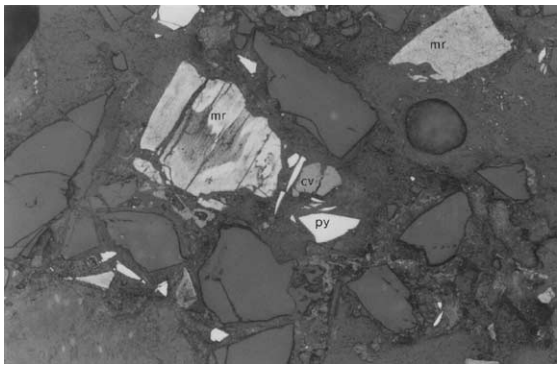

Fig. 14. Photomicrograph in plain reflected light shows secondary covellite-like grains of blue Cu sulfides (cv). Also present are white, homogeneous pyrite (py) and darker, variably heterogeneous pseudomorphs of marcasite (mr) after pyrrhotite. Sample was extracted from a depth of 90 cm. Width of field 0.625 mm.

Jambor, 1990), Heath Steele tailings (Boorman and Watson, 1976; Blowes et al., 1991), Copper Cliff tailings (Coggans et al., 1999), and Nickel Rim tailings (Johnson et al., 2000).

Although the principal candidate for a source of Pb is galena, it was not detected during the mineralogical analysis of the tailings. However, during the field study in 2001, samples of galena up to several cm in length were found in waste-rock piles. Galena was not recovered during mineral processing, and it is therefore likely that most galena was lost to the tailings. Elevated concentrations of Pb were observed in all water samples, with the maximum concentration 8.4 mg L^{-1}. Saturation indices suggest that the pore water becomes saturated with respect to anglesite [$PbSO_4$] where the pH is >3.9. Anglesite was not observed during mineralogical analysis, probably because of the sparseness of galena, but secondary anglesite has been identified in other impoundments and may control Pb concentrations.

Microprobe analyses indicate that magnetite [Fe^{2+}-$Fe^{3+}O_4$], biotite, and amphibole are the likely sources of Cr in the pore water. Another source of Cr could be uvarovite garnet [$Ca_3Cr_2(SiO_4)_3$]; garnet was observed during the mineralogical analysis of the tailings, and a few small crystals were also observed in the waste-rock piles. Froese and Goetz (1981) identified the presence of chromite [$FeCr_2O_4$], Cr-bearing muscovite [$K(Al,Cr)_2AlSi_3O_{10}(OH)_2$], and uvarovite in outcrops in the vicinity of the mine. Dissolved Cr was observed in almost all water samples. Saturation indices indicate that the pore water is undersaturated with respect to all Cr minerals in the MINTEQA2 database. Traces of Cr were observed in Fe oxyhydroxides, suggesting that the oxyhydroxides can be a solid-phase sink for Cr.

4.6.3. Cobalt and As

Microprobe analyses indicate that the main sources of dissolved Co are pyrite and pyrrhotite. Concentrations of Co reach a maximum directly above the hardpan and decrease with depth to below detection limits. Cornell (1991) suggested that Co could be incorporated into the structure of goethite, but Co was not detected in Fe oxyhydroxides within the Camp tailings.

The primary source of As is arsenopyrite, observed as trace amounts within the tailings. In most groundwater conditions, As occurs both as As(III) and As(V) (Smedley and Kinniburgh, 2002). The dominant oxidation state of As in the tailings pore water, expressed in mg L^{-1}, is As(III), and the maximum As(III)/As(V) ratio is 12.3. Arsenic shows a geochemical distribution similar to that of Cu, with the maximum concentration occurring directly above the hardpan, then decreasing sharply at the hardpan interface. Secondary As precipitates were not observed during mineralogical examinations, but As can be attenuated by adsorption onto Fe oxyhydroxides and Fe sulfates (Courtin-Nomade et al., 2003).

5. Conclusions

Sulfide oxidation reactions in the Camp tailings impoundment have consumed nearly all sulfide minerals to a depth of 0.5 m. Oxidation products released from the weathered tailings have resulted in pore waters containing extremely high concentrations of dissolved metals, SO_4, and acid. Carbonate minerals are depleted throughout the vadose zone and well into the water table. The most soluble Al-silicate minerals, i.e., biotite, chlorite, and possibly smectite, are consumed to a 1 m depth near the hardpan layer. The acid front produced from sulfide oxidation has migrated ahead of the oxidation front, consuming the acid-neutralization potential and leaving only the relatively unreactive silicate and Al-silicate minerals. The principal neutralization reactions controlling the pore-water pH and the concentrations of dissolved metals occur at a 1 m depth within the top of the hardpan where there is an abundance of acid neutralization minerals.

Although the Camp tailings have undergone 70 a of sulfide oxidation, the zone of active oxidation has penetrated the tailings to a depth of only 0.5 m. The unsaturated zone is 4.6 m thick, indicating that 4 m of tailings are potentially available to oxidation. When tailings pore water from the vadose zone migrates into the water table, oxidation products can be transported in the groundwater for up to 40 a before discharging to adjacent surface-water bodies. The abundance of sulfide minerals and lack of neutralizing minerals in the tailings suggest that, without the implementation of an effective remedial program, sulfide oxidation in the vadose zone will continue to release acid and elevated concentrations of metals and SO_4 to the tailings pore water for many more decades to centuries.

Acknowledgements

This research was made possible through funding provided by Environment Canada, the Natural Science and Engineering Research Council of Canada, the Toxic Substances Research Initiative managed jointly by Health Canada and Environment Canada, by Manitoba Industry, Trade and Mines, and by Manitoba Conservation. We thank M. Gunsinger, R.G. McGregor, C.H. Talbot, A.E. Brookfield, D. Hatch, J.G. Rajkumar, D. Green, M. Hayashi, and W.D. Robertson for their technical assistance and advice. The authors also thank Franco Frau and an anonymous reviewer for their constructive criticism which greatly improved this manuscript.

References

Al, T.A., Blowes, D.W., 1996. Storm-water hydrograph separation of run off from a mine-tailings impoundment formed by thickened tailings discharge at Kidd Creek, Timmins, Ontario. J. Hydrol. 180, 55–78.

Allison, J.D., Brown, D.S., Novo-Gradac, K.L., 1990. MINTEQA2/PRODEFA2, A Geochemical Assessment Model for Environmental Systems, Version 3.0 User's Manual. Environmental Research Laboratory, Office of Research and Development, US EPA, Athens, GA.

Alpers, C.N., Blowes, D.W., Nordstrom, D.K., Jambor, J.L. 1994. Secondary minerals and acid mine-water chemistry. Jambor, J.L., Blowes, D.W. (Eds.), Environmental Geochemistry of Sulfide Mine-Wastes, Mineral. Assoc. Can. Short Course, 22, pp. 247–270.

Ball, J.W., Nordstrom, D.K., 1991. User's manual for WATEQ4F with revised thermodynamic database and test cases for calculating speciation of major, trace and redox elements in natural waters. US Geol. Surv. Open-File Rep. 91-183.

Banfield, J.F., Eggelton, R.A., 1988. Transmission electron microscope study of biotite weathering. Clays Clay Minerals 36, 47–60.

Barker, J.F., Chatten, S., 1982. A technique for determining low concentrations of total carbonate in geological materials. Chem. Geol. 36, 317–323.

Barker, W.W., Welch, S.A., Chu, S., Banfield, J.F., 1998. Experimental observations of the effects of bacteria on aluminosilicate weathering. Am. Mineral. 83, 1551–1563.

Blowes, D.W., 1990. The geochemistry, hydrogeology, and mineralogy of decommissioned sulfide tailings: a comparative study. PhD Thesis, University of Waterloo, Waterloo, Ont., Canada.

Blowes, D.W., Gillham, R.W., 1988. The generation and quality of streamflow on inactive uranium tailings near Elliot Lake, Ontario. J. Hydrol. 97, 1–22.

Blowes, D.W., Jambor, J.L., 1990. The pore-water chemistry and the mineralogy of the vadose zone of sulfide tailings, Waite Amulet, Quebec. Appl. Geochem. 5, 327–346.

Blowes, D.W., Ptacek, C.J. 1994. Acid neutralization reactions in mine tailings. In: Jambor, J.L., Blowes, D.W. (Eds.), Environmental Geochemistry of Sulfide Mine-Wastes, Mineral. Assoc. Can. Short Course, 22, pp. 271–292.

Blowes, D.W., Reardon, E.J., Jambor, J.L., Cherry, J.A., 1991. The formation and potential importance of cemented layers in inactive sulfide mine tailings. Geochim. Cosmochim. Acta 55, 965–978.

Blowes, D.W., Jambor, J.L., Appleyard, E.C., Reardon, E.J., Cherry, J.A., 1992. Temporal observations of the geochemistry and mineralogy of a sulfide-rich mine-tailings impoundment, Heath Steele Mines, New Brunswick. Explor. Mining Geol. 1, 251–264.

Blowes, D.W., Ptacek, C.J., Jurjovec, J., 2003. Mill tailings: hydrogeology and geochemistry. In: Jambor, J.L., Blowes, D.W., Ritchie, A.I.M. (Eds.), Environmental Aspects of Mine Wastes, Mineral. Assoc. Can. Short Course, 31, pp. 95–116.

Blowes, D.W., Ptacek, C.J., Jambor, J.L., Weisener, C.G., 2003b. The geochemistry of acid mine drainage. In: Lollar, B.S. (Ed.), Environmental Geochemistry. In: Holland, H.D., Turekian, K.K. (Eds.), Treatise on Geochemistry, vol. 9. Elsevier–Pergamon, Oxford, pp. 149–204.

Boorman, R.S., Watson, D.M., 1976. Chemical processes in abandoned sulfide tailings dumps and environmental implications for northeastern New Brunswick. CIM Bull. 69, 86–96.

Braeuning, E., 1977. Mine water development in the lead and zinc deposits of Bawdwin, Burma. In: Second International Symposium on Water–Rock Interaction. Strasbourg, France, pp. 1237–1245.

Chou, I.-M., Seal II, R.R., Hemingway, B.S., 2002. Determination of melanterite–rozenite and chalcanthite–bonattite equilibria by humidity measurements at 0.1 MPa. Am. Mineral. 87, 108–114.

Clarke, F.W., 1916. The Data of Geochemistry, third ed. US Geological Survey Bulletin, vol. 616, p. 1916.

Coggans, C.J., Blowes, D.W., Robertson, W.D., Jambor, J.L., 1999. The hydrogeochemistry of a nickel-mine tailings impoundment – Copper Cliff, Ontario. In: Filipek, L.H., Plumlee, G.S. (Eds.), The Environmental Geochemistry of Mineral Deposits, Part B: Case Studies and Research Topics, Rev. Econ. Geol., 6B, pp. 447–465.

Coleman, R.L., Wallace, B.P., 1978. Tailings disposal in Canada. In: Pickett, D.E. (Ed.), Milling Practice in Canada. CIM Special vol. 16. Can. Inst. Mining Metall. Petrol., Montreal, Canada, pp. 13–20.

Cornell, R.M., 1991. Simultaneous incorporation of Mn, Ni, and Co in the goethite (α-FeOOH) structure. Clay Minerals 26, 427–430.

Courtin-Nomade, A., Bril, H., Neel, C., Lenain, J., 2003. Arsenic in iron cements developed within tailings of a former metalliferous mine – Enguiales, Aveyron, France. Appl. Geochem. 18, 395–408.

Devlin, J.F., 2003. A spreadsheet method of estimating best-fit hydraulic gradients using head data from multiple wells. Ground Water 41, 316–320.

Djingheuzian, L.E., 1957. History of mining in Canada. In: The Milling of Canadian Ores. Authority of the General Committee of the 6th Commonwealth Mining and Metallurgical Congress. Toronto, Canada, pp. 3–36.

Dubrovsky, N.M., Cherry, J.A., Reardon, E.J., 1984. Geochemical evolution of inactive pyritic tailings in the Elliot Lake uranium district. Can. Geotech. J. 22, 110–128.

Environment Canada, 2003. Canadian Climate Normals, 1927–1990, Flin Flon, Manitoba. Accessible at: http://www.climate.weatheroffice.ec.gc.ca/climate_normals.

Farley, W.J., 1949. Geology of the Sherritt Gordon ore body. CIM Bull. 42, 25–30.

Frau, F., 2000. The formation–dissolution–precipitation cycle of melanterite at the abandoned pyrite mine of Genna Luas in Sardinia, Italy: environmental implications. Mineral. Mag. 64, 995–1006.

Freeze, R.A., Cherry, J.C., 1979. Groundwater. Prentice Hall, Englewood Cliffs, NJ.

Froese, E., Goetz, P.A., 1981. Geology of the Sherridon Group in the vicinity of Sherridon, Manitoba. Geol. Surv. Can. Pap. 80-21.

Giere, N.V., Sidenko, E.V., Lazareva, E.V., 2003. The role of secondary minerals in controlling the migration of arsenic and metals from high-sulfide wastes (Berikul gold mine, Siberia). Appl. Geochem. 18, 1347–1359.

Goetz, P.A., Froese, E. 1982. The Sherritt Gordon massive sulfide deposit. Geol. Assoc. Can. Spec. Pap. 25, pp. 557–569.

Goleva, G.A., Polyakov, V.A., Nechayeva, T.P., 1970. Distribution and migration of lead in ground waters. Geochem. Int. 7, 256–268.

Gould, W.D., Kapoor, A. 2003. The microbiology of acid mine drainage. In: Jambor, J.L., Blowes, D.W., Ritchie, A.I.M. (Eds.), Environmental Aspects of Mine Wastes, Mineral. Assoc. Can. Short Course, 31, pp. 203–226.

Hawthorne, F.C., Kennedy, L.P., 1987. A mineralogical study of mine tailings from Farley and Sherridon, northern Manitoba. Phase 1 report. Manitoba Dep. Energy Mines, Winnipeg, Manitoba.

Hvorslev, M.J., 1951. Time lag and soil permeability in groundwater observations. US Army Corps of Engineers, Bull. 36, Waterways Exper. Sta. Corps of Engrs., US Army. Vicksburg, MS, pp. 1–50.

Hydrological Atlas of Canada, 1978. Fisheries and Environment Canada. Surveys and Mapping Branch, Natural Resour. Can., Ottawa.

Jambor, J.L., 1994. Mineralogy of sulfide-rich tailings and their oxidation products. In: Jambor, J.L., Blowes, D.W. (Eds.), Environmental Geochemistry of Sulfide Mine-Wastes, Mineral. Assoc. Can. Short Course, 22, pp. 59–102.

Jambor, J.L., Traill, R.J., 1963. On rozenite and siderotil. Can. Mineral. 7, 751–763.

Jambor, J.L., Nordstrom, D.K., Alpers, C.N., 2000. Metal-sulfate salts from sulfide mineral oxidation. In: Alpers, J.L., Jambor, J.L., Nordstrom, D.K. (Eds.), Sulfate Minerals – Crystallography, Geochemistry, and Environmental Significance, Rev. Mineral. Geochem., 40, pp. 303–350.

Johnson, R.H., Blowes, D.W., Robertson, W.D., Jambor, J.L., 2000. The hydrogeochemistry of the Nickel Rim mine tailings impoundment, Sudbury, Ontario. J. Contam. Hydrol. 41, 49–80.

Jurjovec, J., Ptacek, C.J., Blowes, D.W., 2002. Acid neutralization mechanisms and metal release in mine tailings: A laboratory column experiment. Geochim. Cosmochim. Acta 66, 1511–1523.

Kalinowski, B.E., Schweda, P., 1996. Kinetics of muscovite, phlogopite, and biotite dissolution and alterations at pH 1–4, room temperature. Geochim. Cosmochim. Acta 60, 367–385.

Kamineni, D.C., McGregor, R.G., 1989. A petrographic study of the hardpan samples from selected tailings sites in Manitoba. Atomic Energy of Canada, Pinawa, Ont.

Light, T.S., 1972. Standard solution for redox potential measurements. Anal. Chem. 44, 1038–1039.

Lindgren, W., 1928. Mineral Deposits, third ed. McGraw-Hill, New York.

Malmström, M., Banwart, S., Lewenhagen, L.D., Bruno, J., 1996. The dissolution of biotite and chlorite at 25 °C in the near-neutral pH region. J. Contam. Hydrol. 21, 201–213.

McGregor, R.G., Blowes, D.W., 2002. The physical, chemical, and mineralogical properties of three cemented layers within sulfide-bearing mine tailings. J. Geochem. Explor. 76, 195–207.

Meloy, T.P., 1962. The treatment of fine particles during flotation. In: Furstenau, D.W. (Ed.), Froth Flotation 50th Anniversary Volume. Am. Inst. Mining Metall. Petrol. Eng., New York, pp. 247–257.

Mineral Resources Branch, 1978. Sherridon Mine Reference-Manitoba Card #839. A Compendium. Natural Resour. Can., Ottawa.

Moncur, M.C., Ptacek, C.J., Blowes, D.W., Jambor, J.L., 2003. Fate and transport of metals from an abandoned tailings impoundment after 70 years of sulfide oxidation. In: Graeme, S., Beckett, P., Conroy, H. (Eds.), Proceedings of Sudbury '03, Mining and the Environment III. Laurentian University, Sudbury, Ont., pp. 238–247.

Murakami, T., Utsunomiya, S., Yokoyama, T., Kasama, T., 2003. Biotite dissolution processes and mechanisms in the laboratory and in nature: Early stage weathering environments and vermiculitization. Am. Mineral. 88, 377–386.

Nordstrom, D.K., 1977. Thermochemical redox equilibria in Zobell's solution. Geochim. Cosmochim. Acta 41, 1835–1841.

Nordstrom, D.K., 1982. Aqueous pyrite oxidation and the consequent formation of secondary minerals. In: Kittrick, A., Fanning, D.S., Hossner, L.R. (Eds.), Acid Sulphate Weathering, Soil Sci. Soc. Am. Spec. Pub. 10, pp. 37–56.

Nordstrom, K.D., Alpers, C.N., 1999. Geochemistry of acid mine waters. In: Plumlee, G.S., Logsdon, M.J. (Eds.), The Environmental Geochemistry of Mineral Deposits. Part A: Processes, Techniques, and Health Issues, Rev. Econ. Geol., 6A, pp. 133–160.

Nordstrom, K.D., Jenne, E.A., Ball, J.W., 1979. Redox equilibria of iron in mine waters. In: Jenne, E.A. (Ed.), Chemical Modeling in Aqueous Systems, Am. Chem. Soc. Symp. Ser., 93, pp. 51–79.

Nordstrom, K.D., Alpers, C.N., Ptacek, C.J., Blowes, D.W., 2000. Negative pH and extremely acidic mine waters from iron mountain, California. Environ. Sci. Technol. 34, 254–258.

Patterson, R.J., Frape, S.K., Dykes, L.S., McLeod, R.A., 1978. A coring and squeezing technique for the detailed study of subsurface water chemistry. Can. J. Earth Sci. 15, 162–169.

Plummer, L.N., Parkhurst, D.L., Fleming, G.W., Dunkle, S.A., 1988. A computer program incorporating Pitzer's equations for calculation of geochemical reactions in brines. US Geol. Surv. Water Resour. Investig. Rep. 88-4153.

Plummer, L.N., Michel, R.L., Thurman, E.M., Glynn, P.D., 1993. Environmental tracers for age dating young ground water. In: Ally, W.M. (Ed.), Regional Ground-Water Quality. Van Nostrand Reinhold, New York, pp. 72–111.

Ptacek, C.J, 1992. Experimental determination of siderite solubility in high ionic-strength aqueous solutions. PhD Thesis, University of Waterloo, Waterloo, Ontario.

Ptacek, C.J., Blowes, D.W., 2000. Predicting SO_4-mineral solubility in concentrated waters. In: Alpers, C.N., Jambor, J.L., Nordstrom, D.K. (Eds.), Sulfate Minerals – Crystallography, Geochemistry, and Environmental Significance, Rev. Mineral. Geochem., 40, pp. 513–540.

Ptacek, C.J., Blowes, D.W., 2003. Geochemistry of concentrated waters In: Jambor, J.L., Blowes, D.W., Ritchie, A.I.M. (Eds.), Environmental Aspects of Mine Wastes, Mineral. Assoc. Can. Short Course, 31, pp. 239–525.

Ptacek, C.J., Moncur, M.C., McGregor, R.G., Blowes, D.W., 2001. Geochemical controls on metal concentrations in mine tailings that have undergone 50 years of oxidation. In:

11th Annual V.M. Goldschmidt Conference. Contribution No. 1088, Lunar Planet. Inst., Houston, TX, Abstract #3647 (CD-ROM).

Pyatt, F.B., Grattan, P.J., 2001. Some consequences of ancient mining activities on the health of ancient and modern human populations. J. Pub. Health Med. 23, 235–236.

Pyatt, F.B., Gilmore, G., Grattan, P.J., Hunt, C.O., McLeren, S., 2000. An imperial legacy? An exploration of the environmental impacts of ancient metal mining and smelting in Southern Jordan. J. Archaeol. Sci. 27, 771–778.

Robertson, W.D., Cherry, J.C., 1989. Tritium as an indicator of recharge and dispersion in a groundwater system in central Ontario. Water. Resour. Res., 1111–1123.

Rufe, E., Hochella Jr., M.F., 1999. Quantitative assessment of reactive surface area of phlogopite during acid dissolution. Science 285, 875–876.

Smedley, P.L., Kinniburgh, D.G., 2002. A review of the source, behavior, and distribution of arsenic in natural waters. Appl. Geochem. 17, 517–568.

Standard Methods for the Examination of Water and Wastewater (SMEWW), 1992. American Health Association, Washington, DC.

Smyth, D.J.A., 1981. Hydrology and geochemical studies above the water table in an inactive uranium impoundment near Elliot Lake, Ontario. M.Sc. Project, University of Waterloo, Waterloo, Ontario.

Starr, R.C., Ingleton, R.A., 1992. A new method for collecting core samples without a drill rig. Ground Water Monit. Remed. 41, 91–95.

Tassé, N., Germain, D., Dufour, C., Tremblay, R., 1997. Hardpan formation in the Canadian Malartic mine tailings: implications for the reclamation of the abandoned impoundment. In: Fourth International Conference on Acid Rock Drainage. CANMET, Natural Resour. Can., Ottawa, vol. 4, pp. 1797–1812.

Taylor, A.S., Blum, J.D., Lasaga, A.C., MacInnis, I.N., 2000. Kinetics of dissolution and Sr release during biotite and phlogopite weathering. Geochim. Cosmochim. Acta 64, 1191–1208.

Vukovic, M., Soro, A., 1992. Determination of Hydraulic Conductivity of Porous Media from Grain-Size Composition. Water Resources Publications, Littleton, Colorado.

Walker, G.B., 1930. Report No. 353, Flotation test on ore samples from Sherritt-Gordon Mines, Ltd., Sherridon, Manitoba. Investigations in Ore Dressing and Metallurgy. Dept. Mines Rep. 724. Natural Resources Canada, Ottawa.